



January 2014

Investigation Of Marine Stratocumulus Under Coupled And Decoupled Conditions Over The Arm Azores Site

Adam Christopher Schwantes

Follow this and additional works at: <https://commons.und.edu/theses>

Recommended Citation

Schwantes, Adam Christopher, "Investigation Of Marine Stratocumulus Under Coupled And Decoupled Conditions Over The Arm Azores Site" (2014). *Theses and Dissertations*. 1710.
<https://commons.und.edu/theses/1710>

This Thesis is brought to you for free and open access by the Theses, Dissertations, and Senior Projects at UND Scholarly Commons. It has been accepted for inclusion in Theses and Dissertations by an authorized administrator of UND Scholarly Commons. For more information, please contact zeinebyousif@library.und.edu.

INVESTIGATION OF MARINE STRATOCUMULUS UNDER COUPLED AND
DECOUPLED CONDITIONS OVER THE ARM AZORES SITE

by

Adam Christopher Schwantes
Bachelor of Science, Northland College, 2012

A Thesis
Submitted to the Graduate Faculty

of the

University of North Dakota
in partial fulfillment of the requirements

for the degree of
Master of Science

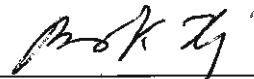
Grand Forks, North Dakota
December
2014

Copyright 2014 Adam Schwantes

This thesis, submitted by Adam Schwantes in partial fulfillment of the requirements for the Degree of Master of Science from the University of North Dakota, has been read by the Faculty Advisory Committee under whom the work has been done, and is hereby approved.



Xiquan Dong

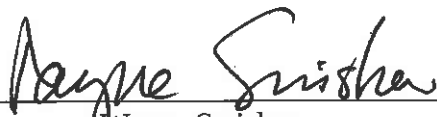


Baiké Xi



Mark Askelson

This thesis is being submitted by the appointed advisory committee as having met all of the requirements of the Graduate School at the University of North Dakota and is hereby approved.



Wayne Swisher
Dean of the Graduate School



Date

PEMISSION

Title Investigation of Marine Stratocumulus Under Coupled and Decoupled Conditions Over the ARM Azores Site

Department Atmospheric Sciences

Degree Master of Science

In presenting this thesis in partial fulfillment of the requirements for a graduate degree from the University of North Dakota, I agree that the library of this University shall make it freely available for inspection. I further agree that permission for extensive copying for scholarly purposes may be granted by the professor who supervised my thesis work or, in his absence, by the Chairperson of the department or the dean of the Graduate School. It is understood that any copying or publication or other use of this thesis or part thereof for financial gain shall not be allowed without my written permission. It is also understood that due recognition shall be given to me and to the University of North Dakota in any scholarly use which may be made of any material in my thesis.

Signature Adam Schwes

Date 11/07/2014

TABLE OF CONTENTS

LIST OF FIGURES.....	viii
LIST OF TABLES.....	xii
ACKNOWLEDGEMENTS	xiii
ABSTRACT.....	xiv
CHAPTER	
I. INTRODUCTION.....	1
Mean Meteorological Conditions over the Azores.....	2
Marine Boundary Layer.....	3
Stratocumulus Life Cycle.....	4
Stratocumulus Cloud Maintenance.....	6
Radiative Forcings.....	6
Turbulence.....	7
Surface Fluxes.....	9
Precipitation.....	10
Recent Studies.....	10
II. DATA.....	15
Observations.....	15
Microwave Radiometer.....	16
Balloon Borne Sounding System/ Merged Soundings.....	17
W-Band (95 GHz) ARM Cloud Radar.....	18

	Aerosol Observing System.....	19
	Vaisala Ceilometer.....	20
	NASA LARC Satellite Products (Meteosat-9)	20
	Retrieved MBL cloud micro-physical properties from the ARM AMF dataset.....	21
	Cloud droplet effective radius (re).....	21
	Cloud droplet number concentration (N).....	21
III.	METHODOLOGY.....	23
	Case Selection.....	23
	Potential Temperature Method.....	23
	Comparison of Potential Temperature Method to Similar Methods.....	27
	Lifting Condensation Level Method.....	27
	Comparison between LCL and Potential Temperature Methods.....	28
	Drizzle vs Non-Drizzle.....	28
	Day vs Night.....	29
	Statistical Testing.....	29
IV.	RESULTS/DISCUSSION.....	32
	Cases Selected.....	32
	MBL cloud properties	33
	Statistics.....	53
	Coupled vs Decoupled.....	53
	Drizzle vs Non-Drizzle.....	59

	Day vs Night.....	66
	Stratocumulus Cloud Layer Lifetime.....	71
	Satellite Images.....	72
V.	CONCLUSIONS.....	78
VI.	REFERENCES.....	81

LIST OF FIGURES

Figure	Page
1.	Azores High during the summer located south of the Azores Islands.....2
2.	Schematic showing the key processes occurring in a stratocumulus-topped boundary layer. The downward arrow for turbulent mixing represents air that is sinking due to radiative cooling at the cloud top, while the upward arrow for turbulent mixing represents rising air caused by the warming of the ocean surface. From Wood (2012).....5
3.	Satellite image of stratocumulus clouds off the coast of Peru (Courtesy of Wood class presentation).....6
4.	“Schubert” diagrams with (a) and (b) indicating typical air parcel circuits and (c) buoyancy profiles through a stratocumulus topped boundary layer that is well mixed. (a) and (b) show liquid water mixing ratio and virtual potential temperature circuits. Wavy dashed lines indicate heights of updraft and downdraft condensation levels respectively and inversion height. (Courtesy of Wood 2012 Figure 21).....8
5.	Map showing the location of Graciosa Island with respect to the North Atlantic and Europe. Provided by Google Maps.....15
6.	Potential temperature profiles for a well mixed boundary layer (b) and a decoupled boundary layer (a).....24
7.	Water vapor mixing ratio profiles for a well mixed boundary layer (b) and a decoupled boundary layer (a).....26
8.	Radar reflectivity for November 2-3, 2009. Red line represents the best estimate cloud base, which uses MPL and VCEIL measurements.....29
9.	Time series of (a) radar reflectivity, (b) cloud-base (Z_b) and -top (Z_t) heights derived from ARM radar-lidar measurements, (c) cloud liquid water path (LWP) retrieved from microwave radiometer, (d) cloud-droplet effective radius (r_e) (e) cloud droplet number concentration (N_d) and cloud condensation nuclei concentration (N_{CCN}) under coupled and decoupled conditions during the November 22-23 2009 case..... 35

10.	Normalized profiles of (a) temperature, (b) LWC, and (c) r_e , for the November 22-23,2009 case.....	36
11.	Time series of (a) radar reflectivity, (b) cloud-base (Zb) and –top (Zt) heights derived from ARM radar-lidar measurements, (c) cloud liquid water path (LWP) retrieved from microwave radiometer, (d) cloud-droplet effective radius (r_e) (e) cloud droplet number concentration (N_d) and cloud condensation nuclei concentration (N_{CCN}) under coupled and decoupled conditions during the May 11-12, 2010 case.....	38
12.	As in Fig. 11, but for hourly satellite images within a grid box of .5°X.5° centered on the ARM Azores site (with symbol A).....	39
13.	Normalized profiles of (a) temperature, (b) LWC, and (c) r_e , for the May 11-12, 2010 case.....	39
14.	Time series of (a) radar reflectivity, (b) cloud-base (Zb) and –top (Zt) heights derived from ARM radar-lidar measurements, (c) cloud liquid water path (LWP) retrieved from microwave radiometer, (d) cloud-droplet effective radius (r_e) (e) cloud droplet number concentration (N_d) and cloud condensation nuclei concentration (N_{CCN}) under coupled and decoupled conditions during the October 2-4, 2010 case.....	42
15.	Normalized profiles of (a) temperature, (b) LWC, and (c) r_e , for the October 2-4, 2010 case.....	43
16.	Time series of (a) radar reflectivity, (b) cloud-base (Zb) and –top (Zt) heights derived from ARM radar-lidar measurements, (c) cloud liquid water path (LWP) retrieved from microwave radiometer, (d) cloud-droplet effective radius (r_e) (e) cloud droplet number concentration (N_d) and cloud condensation nuclei concentration (N_{CCN}) under coupled and decoupled conditions during the October 21-22, 2009 case.....	45
17.	Normalized profiles of (a) temperature, (b) LWC, and (c) r_e , for the October 21-22, 2009 case.....	46
18.	Time series of (a) radar reflectivity, (b) cloud-base (Zb) and –top (Zt) heights derived from ARM radar-lidar measurements, (c) cloud liquid water path (LWP) retrieved from microwave radiometer, (d) cloud-droplet effective radius (r_e) (e) cloud droplet number concentration (N_d) and cloud condensation nuclei concentration (N_{CCN}) under coupled and decoupled conditions during the November 2-3, 2009 case.....	47
19.	Normalized profiles of (a) temperature, (b) LWC, and (c) r_e , for the November 2-3, 2009 case.....	48

20.	Time series of (a) radar reflectivity, (b) cloud-base (Z_b) and –top (Z_t) heights derived from ARM radar-lidar measurements, (c) cloud liquid water path (LWP) retrieved from microwave radiometer, (d) cloud-droplet effective radius (r_e) (e) cloud droplet number concentration (N_d) and cloud condensation nuclei concentration (N_{CCN}) under coupled and decoupled conditions during the November 7-9, 2010 case.....	49
21.	Normalized profiles of (a) temperature, (b) LWC, and (c) r_e , for the November 7-9, 2010 case.....	50
22.	Time series of (a) radar reflectivity, (b) cloud-base (Z_b) and –top (Z_t) heights derived from ARM radar-lidar measurements, (c) cloud liquid water path (LWP) retrieved from microwave radiometer, (d) cloud-droplet effective radius (r_e) (e) cloud droplet number concentration (N_d) and cloud condensation nuclei concentration (N_{CCN}) under coupled and decoupled conditions during the October 11-12, 2010 case.....	51
23.	Normalized profiles of (a) temperature, (b) LWC, and (c) r_e , October 11-12, 2010 case.....	52
24.	PDFs and CDFs of the coupled (blue) and decoupled (red) stratocumuli macrophysical properties for all cases.....	55
25.	PDFs and CDFs of the coupled (blue) and decoupled (red) stratocumuli microphysical properties for all cases.....	57
26.	PDFs and CDFs of the coupled(blue)/decoupled(red) non-drizzling (left) and drizzling (right) stratocumuli macrophysical properties for all cases.....	61
27.	PDFs and CDFs of the coupled(blue)/decoupled(red) non-drizzling (left) and drizzling (right) stratocumuli microphysical properties for all cases.....	64
28.	PDFs and CDFs of the coupled (blue)/decoupled (red) day (left) and night (right) stratocumuli macrophysical properties for all cases.....	67
29.	PDFs and CDFs of the coupled (blue)/decoupled (red) day (left) and night (right) stratocumuli microphysical properties for all cases.....	70
30.	Hourly total cloud fraction images taken from Meteosat-9 over the Azores (A) on October 11, 2010.....	73
31.	Hourly total cloud fraction images taken from Meteosat-9 over the Azores (A) on October 12, 2010.....	74

32.	Hourly total cloud fraction images taken from Meteosat-9 over the Azores (A) on October 13, 2010.....	75
33.	Hourly total cloud fraction images taken from Meteosat-9 over the Azores (A) on October 14, 2010.....	76

LIST OF TABLES

Table	Page
1. The vertical resolution for all Mergesonde altitude levels.....	18
2. Uncertainties of instruments/methods used in this study.....	22
3. List of cases chosen.....	32
4. Mean values of different cloud properties for coupled and decoupled stratocumuli.....	58
5. Median values of different cloud properties for coupled and decoupled stratocumuli.....	58
6. Standard deviation values of different cloud properties for coupled and decoupled stratocumuli.....	59
7. Mean and standard deviation values of different cloud properties for drizzling and non-drizzling stratocumuli.....	65
8. Mean and standard deviation values of different cloud properties for daytime and nighttime stratocumuli.....	71

ACKNOWLEDGEMENTS

I'd first like to thank my advisors Drs. Xiquan Dong and Baike Xi for helping guide my research for the past two years. Without their patience and sound advice, this thesis work would not be possible. I'd also like to thank them for making it financially possible through a NASA grant to pursue my master's degree, which would have been impossible without their help. I'd also like to thank my other committee member Dr. Mark Askelson for helping me to revise my thesis and for being a great teacher and friend for the past two years.

I would also like to thank all my friends and family for all of the support they have given me the past two years. Without them, this thesis work would not have been possible.

Finally I'd like to thank God for giving me the strength and skills to complete this thesis work, and for always being a source of comfort.

ABSTRACT

Stratocumuli are a type of low clouds composed of individual convective elements that together form a continuous layer of clouds. Stratocumuli cover large regions of the Earth's surface, which make them important components in the Earth's radiation budget. Stratocumuli strongly reflect solar shortwave radiation, while weakly affecting outgoing longwave radiation. This leads to a strong radiative cooling effect that affects the Earth's radiation budget. Therefore it is important to investigate the mechanisms that affect the longevity of stratocumuli, so that their impact on the Earth's radiation budget can be fully understood. One mechanism that is currently being studied as influencing the lifetime of such cloud layers is boundary layer/surface coupling. It has been shown that in some regions (i.e. the west coast of South America) stratocumuli tend to break up when the boundary layer is decoupled with the surface, because they are cut off from their moisture source. This study will investigate the macro- and micro-physical properties of stratocumuli when boundary layers are either coupled to or decoupled from the surface. This will help advance understanding of the effects these macro- and micro-physical properties have on the lifetime of stratocumuli under different boundary layer conditions.

This study used the Department of Energy Atmospheric Radiation Measurement (DOE ARM) mobile measurements facility (AMF) at the Azores site from June 2009 to December 2010. The measurements that were used include temperature profiles from radiosondes, cloud liquid water path (LWP) retrieved from the Microwave radiometer,

and cloud base and top heights derived from W-band ARM Cloud Radar and lidar. Satellite images provided by the NASA Langley Research Center were also used to visually decipher cloud types over the region so that only single-layered stratocumuli cases are used in the study. To differentiate between coupled and decoupled cloud layers, two methods are used. The first method compares cloud base height and lifting condensation level (LCL) for surface air parcels. The second method uses potential temperature profiles to indicate whether a boundary layer is coupled or decoupled from the surface. The results from these two methods were then compared using select cases/samples when both methods classified a sample as coupled or decoupled. In this study, a total of seven coupled or decoupled cases (2-3 days long each) have been selected from the 19 month AMF dataset.

Characteristics of the coupled and decoupled cases have been studied to identify similarities and differences. Furthermore, comparison results from this study have shown that there are similarities and differences between drizzling/non-drizzling stratocumulus clouds and decoupled/coupled stratocumulus clouds. Drizzling/decoupled stratocumuli tend to have higher LWP, cloud-droplet effective radius (r_e), cloud-top height, and cloud thickness values while non-drizzling/coupled stratocumuli have higher cloud-droplet number concentration (N_d) and cloud condensation nuclei concentration (N_{CCN}) values. It was also determined that during daytime hours when stratocumuli are decoupled, they tend to be open cells, while coupled stratocumuli tend to be closed cells. Finally, decoupled nighttime stratocumuli were found to have higher LWPs compared to decoupled daytime stratocumuli, which resulted in the significant amount of heavy drizzle events occurring at night.

CHAPTER I

Introduction

Marine Boundary Layer (MBL) stratocumulus clouds are a genus of low-level clouds consisting of many individual convective elements that together form a layer. Stratocumuli cover enormous regions of the Earth's surface and exhibit a variety of structures over a wide range of spatial scales. They cover approximately 23% of the ocean and 12% of the land surface, making them the dominant cloud type in terms of area covered (Warren et al. 1986, 1988; Hahn and Warren 2007). Stratocumulus clouds strongly reflect incoming shortwave (SW) radiation (Chen et al. 2000) and weakly affect outgoing longwave radiation (OLR) resulting in a strong negative net radiation effect on the Earth's surface (Stephens and Greenwald 1991; Hartmann et al. 1992). Small changes in either the coverage or thickness of stratocumuli can produce a radiative effect comparable to that of increasing greenhouse gases (Hartmann and Short 1980; Randall et al. 1984; Slingo 1990). Understanding how, when, and where stratocumuli form and quantifying their properties, therefore, constitute important atmospheric phenomena that need to be understood so that the Earth's radiation budget can be better understood. Recent studies (Woods 2012, Jones et al. 2011, Remillard et al. 2012, Logan et al. 2014, Dong et al. 2014a, Xi et al. 2014) have shown that interactions between the Earth's surface and stratocumuli along with drizzle are key factors that control the macro- and micro-physical properties of stratocumulus clouds. The purpose of this study is to investigate the similarities and differences of macro- and micro-physical properties of stratocumuli between

coupled and decoupled cases and under different atmospheric conditions including drizzle/non-drizzle and day/night. This study will help advance understanding of the effects of different atmospheric conditions on the microphysical properties and persistence of stratocumulus clouds. Herein, stratocumulus clouds over the Azores are studied.

A. Mean Meteorological conditions over the Azores

In this section the meteorological conditions over the Azores are discussed. The average synoptic conditions over the Azores are shown in Figure 1. The synoptic conditions over the Azores are dominated by the Azores High during the summer and fall seasons. The Azores High (also known as the North Atlantic High, the Bermuda-Azores High, or the Bermuda High) is a semi-permanent large subtropical center of high atmospheric pressure typically found south of the Azores in the Atlantic Ocean, at the Horse (30° N) latitudes.

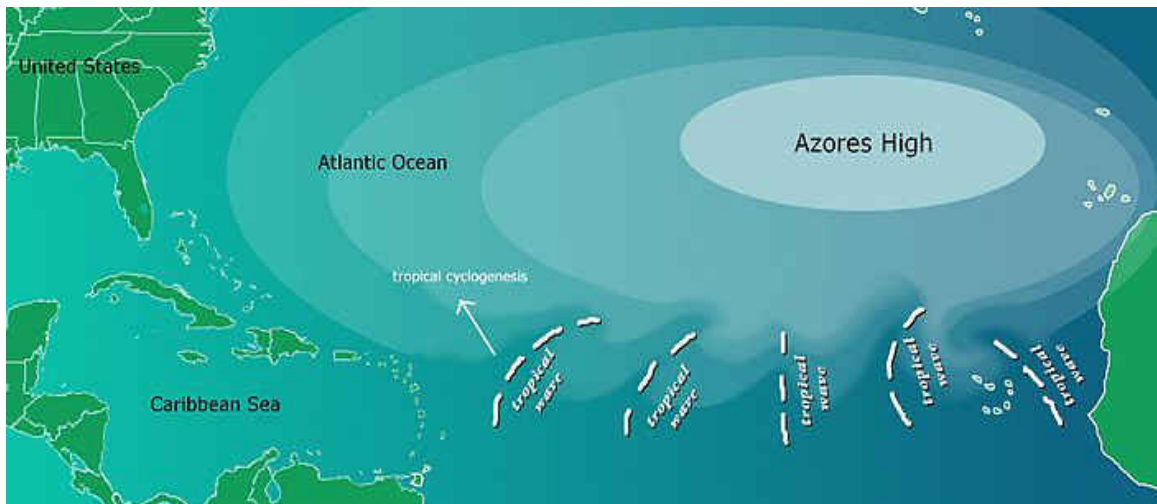


Figure 1. The Azores High during the summer located south of the Azores Islands.

The Azores High forms one pole of the of the North Atlantic oscillation, with the other being the Icelandic Low. This system has widespread influence over the weather and climatic patterns over vast areas of North Africa and Europe, and favors the

development of marine boundary layer (MBL) clouds. During the winter and spring months, the Azores High moves south allowing a low pressure system to dominate the region, which provides a more favorable environment for cumulus growth rather than stable stratocumuli (Remillard et al. 2012, Dong et al. 2014a).

B. Marine Boundary Layer (MBL)

The vertical and horizontal structures of stratocumulus are strongly tied to the vertical structure of the boundary layer. The fractional coverage of low-level clouds is greatest when the stratocumulus topped boundary layer (STBL) depth (z) is shallow ($0.5 < z < 1.0$) and these STBLs are often well-mixed (Fig. 2a). Variables such as wind, mixing ratio, and potential temperature are constant with height in a well mixed STBL. Well mixed STBLs are also capped by a strong temperature inversion just above the cloud layer.

As the STBL deepens beyond 1 km (Figure 2b), usually due the entrainment of free-tropospheric air into the STBL, it becomes difficult for longwave (LW) cooling (discussed in the next section) at the cloud-top to sustain mixing of positively buoyant entrained air over the entire depth of the STBL (Wood 2012). The STBL then begins to separate into two layers with the upper layer becoming decoupled from the surface moisture supply. Within a decoupled STBL, the stratocumulus layer is often within a well-mixed layer, but the negatively buoyant eddies created by the LW cooling are not strong enough to mix with the sub-cloud boundary layer. Meanwhile, the near surface layer can be well mixed due to the surface turbulence. Above this near-surface layer, cumulus clouds tend to form, which further decouple the stratocumulus cloud layer from the surface.

The STBL is capped by a shallow layer over which there are strong gradients in potential temperature, humidity, and radiative cooling rates. This layer is commonly referred to as the inversion layer and is typically no more than a few tens of meters thick. The top of this inversion layer is not as well defined as the base, with relatively weak vertical gradients relaxing to free tropospheric air. This is in contrast to the sharp temperature gradients at the base of the inversion layer, which is usually located just above the cloud top due to the LW radiative cooling at the cloud top. The strength and location of this inversion layer greatly affect the cloud top entrainment rate of free tropospheric air (Wood 2012).

C. Stratocumulus Life-Cycle

MBL stratocumuli are formed by weak, shallow convective currents, potentially triggered by turbulent airflows aloft. This shallow layering is enabled through capping by a temperature inversion, which is typically only tens of meters thick. MBL stratocumulus clouds are defined as low level clouds whose dynamics are primarily driven by convective instabilities caused by cloud top radiative cooling, which then distinguishes them from stratus clouds. Figure 2 shows a schematic of the key processes that occur in a stratocumulus topped boundary layer. The downward arrow for turbulent mixing in Figure 2 represents air that is sinking due to radiative cooling at the cloud top, while the upward arrow for turbulent mixing represents rising air caused by the warming of the ocean surface.

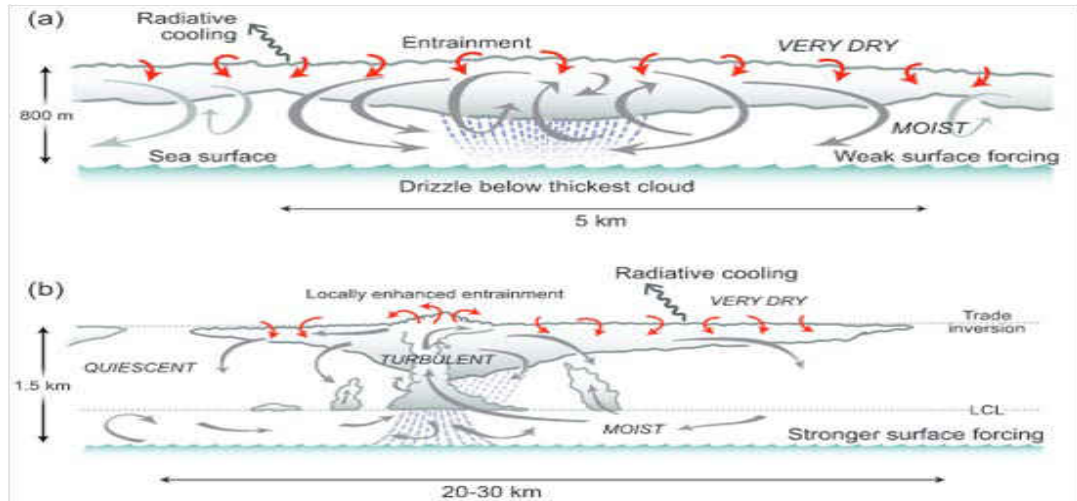


Figure 2. Schematic showing the key processes occurring in a stratocumulus-topped boundary layer. The downward arrow for turbulent mixing represents air that is sinking due to radiative cooling at the cloud top, while the upward arrow for turbulent mixing represents rising air caused by the warming of the ocean surface. From Wood (2012)

Once this circulation is established, moisture is transported from the surface to the stratocumulus layer. This circulation helps to maintain the stratocumulus layer and keep it closed cell, meaning there are no cloud breaks within the stratocumulus layer (Fig. 3). During the day, shortwave (SW) heating negates the LW cooling at the cloud top, which weakens the circulation between the stratocumulus layer and the surface, thus splitting the circulation into two separate smaller circulations; one circulation within the cloud and a secondary circulation between the cloud base and surface. Once this circulation is cut-off, the stratocumulus layer begins to break apart and becomes open celled, meaning there are cloud breaks present within the stratocumulus layer (Fig. 3).

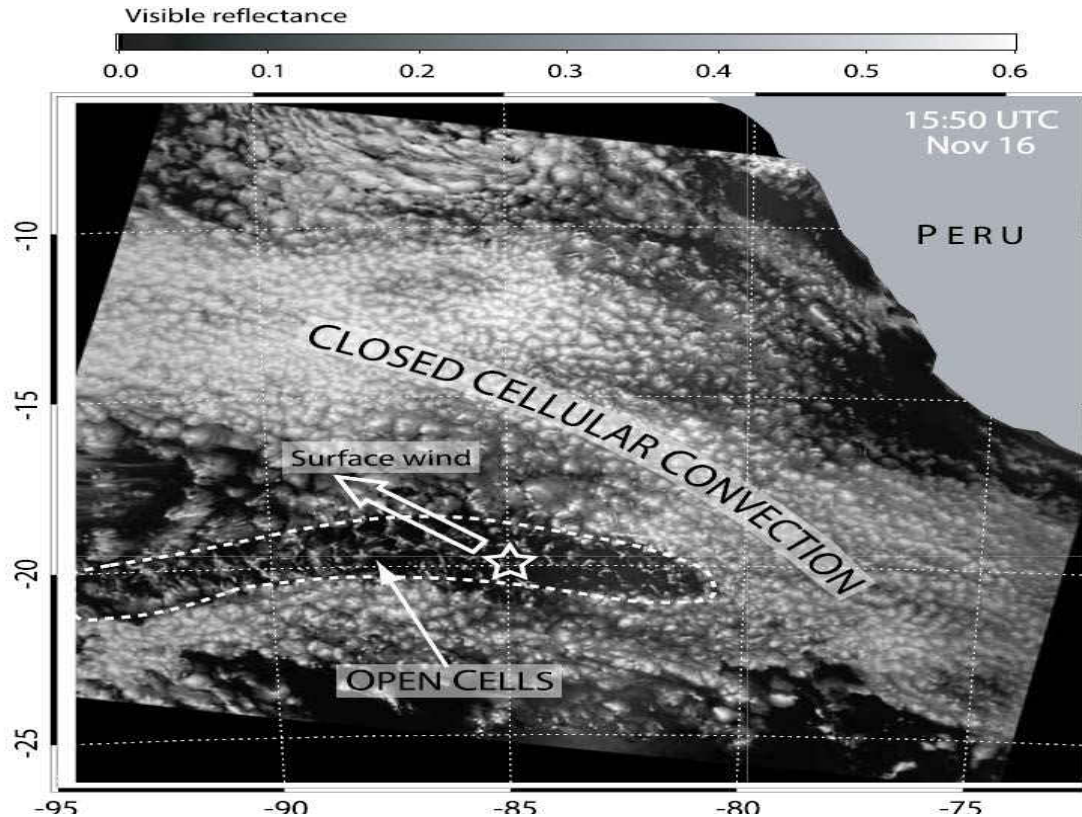


Figure 3. Satellite image of stratocumulus clouds off the coast of Peru. (Courtesy of Wood class presentation)

D. Stratocumulus Cloud Maintenance

MBL stratocumulus clouds are driven by several atmospheric processes which include radiative forcing, turbulence, surface fluxes, latent heat release, and entrainment. Over the ocean, precipitation also plays a key role in regulating stratocumulus clouds. Each of these forcings are in detail in this section.

1. Radiative forcing

LW radiative cooling at cloud top is the primary cause of convection in stratocumulus, particularly during the nighttime. During the day, the cloud layer is warmed by absorption of solar radiation, which partially offsets the LW cooling that occurs at the cloud top. Over longer time periods, stratocumulus clouds can impact the

radiation budgets at the top of the atmosphere (TOA) and at the surface. In particular, stratocumulus clouds help to maintain cool ocean surfaces. Liquid water droplets within the cloud layer scatter and absorb radiation depending on wavelength, droplet size, and droplet concentration. Although scattering is important at all wavelengths across the visible and infrared spectrum, absorption dominates in the infrared and near infrared wavelengths.

2. Turbulence

The mean state of stratocumulus clouds is determined directly by fluxes of energy and water, and indirectly by other atmospheric constituents such as aerosols. The main fluxes that drive stratocumulus clouds are predominantly turbulent. The strength of these turbulent wind field components, particularly the vertical component, influence the amount of free-tropospheric air entrained into the stratocumulus cloud layer.

Vertical turbulent energy and moisture flux profiles are important for determining stratocumulus cloud properties. These fluxes are defined in Lilly (1968) as the mixed layer theory, which describes the vertical structure of the fluxes necessary to maintain a well mixed layer given the different forces applied to it. For a layer to be well mixed, the vertical energy and moisture fluxes must be linear functions of height. Precipitation and cloud droplet sedimentation, however, can contribute to moisture transport (Woods 2005), especially in thick stratocumuli. Within the cloud layer the vertical turbulent flux of liquid water is an important contributor to the total water flux (Nicholls 1984; Duynkerke et al 1995).

Under most circumstances, the buoyancy flux is the primary source of turbulent kinetic energy in the (STBL). Buoyancy flux peaks within the cloud layer, with smaller

values located in the subcloud layer. The large buoyancy fluxes found within the cloud layer are primarily caused by radiative cooling and are enhanced by latent heating effects. For mixed layers, there is a sharp increase in the buoyancy flux above the cloud base due to latent heat release (Lilly 1968). This can be illustrated using ‘Schubert’ circuit diagrams (Schubert et al. 1979a) (Fig. 4).

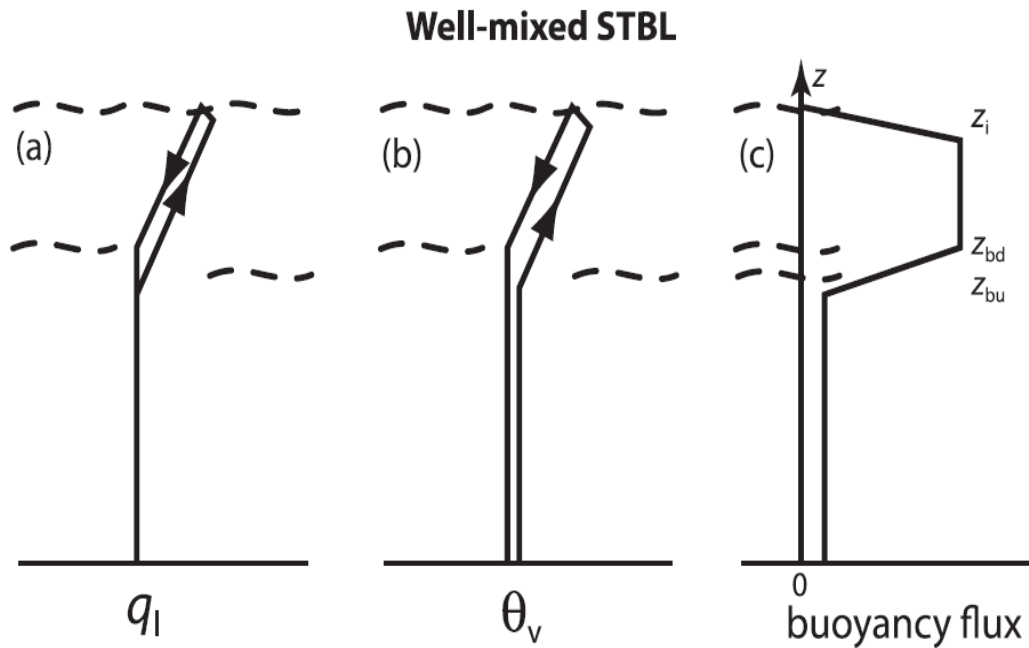


Figure 4. “Schubert” diagrams with (a) and (b) indicating typical air parcel circuits and (c) buoyancy profiles through a STBL that is well mixed. (a) and (b) show liquid water mixing ratio and virtual potential temperature circuits. Wavy dashed lines indicate heights of updraft and downdraft condensation levels respectively and inversion height. (Courtesy of Wood 2012 Figure 21)

In stratocumulus layers, updrafts are warmer, and more positively buoyant than the cooler downdrafts (Fig. 4), which constitute the source of buoyant turbulence production. The asymmetry, which is seen in the differences between upward and downward moving branches of the circulation at the cloud base, is primarily driven by the differences in liquid water content (LWC) between upward and downward moving parcels (Fig. 4a). At the top of the circuit, radiative cooling forces the rising parcel to

become negatively buoyant while entrainment evaporates some of the liquid water, making the downdrafts drier than the updrafts (Figs. 4a, b). With small supersaturations (<1%) in the cloud layer, the liquid water flux is therefore primarily governed by the vertical flux of water vapor into the cloud layer.

During the daytime when solar radiation reduces the intensity of cloud top cooling, or when cloud top entrainment warming and drying is strong enough to raise the lifting condensation level (LCL) for downward moving parcels, the virtual potential temperature at the LCL is greater than in the sub-cloud layer. In this case, the buoyancy flux is negative below the stratocumulus cloud base (Nicholls and Leighton 1986), resulting in a turbulence sink that leads the stratocumulus layer to becoming decoupled from the surface (Turton and Nicholls 1987).

3. Surface Fluxes

The surface latent heat flux (LHF) provides the primary source of moisture in most STBLs. The surface LHF is determined by the surface relative humidity (RH), the surface temperature, and surface wind speeds. (Hartmann 1994) The surface RH depends upon the processes controlling the STBL moisture and temperature budgets, primarily surface precipitation and entrainment. This is also true for surface sensible heat flux (SHF), although in most marine STBLs the SHF is a weak source of turbulence compared to LW cooling for the following two reasons: (1) due to the high heat capacity of the ocean, the ocean surface does not warm quickly, and (2) if stratocumulus clouds have a long enough lifetime, they will cool the surface.. In well-mixed STBLs, particularly over warm oceans, the surface LHF is an important source of buoyant turbulent kinetic energy production, making it a key process affecting internal STBL dynamics (Wood 2012).

4. Precipitation

Marine stratocumulus clouds frequently produce light precipitation, usually in the form of drizzle. Drizzle, normally defined as having radar reflectivity higher than -17 dBZ (Frisch et al. 1995) is found 20-40% of the time in regions of persistent marine stratocumulus clouds (Leon et al. 2008; Wood et al. 2009a). The effects of drizzle on the STBL are complex. First, drizzle warms the cloud layer, stabilizing the STBL, which in turn reduces turbulent mixing and induces stratification. Second, drizzle evaporates below the cloud base, due to the small size of drizzle droplets (30- 100 μ m). This evaporation can lead to decoupling of the stratocumulus cloud layer from the surface, and can also lead to closed celled stratocumuli becoming open celled stratocumuli.

E. Recent Studies

Previous field experiments focusing on marine stratocumulus clouds include the Atlantic Stratocumulus Transition Experiment (ASTEX) (Albrecht et al 1995), the East Pacific Investigation of Climate (EPIC) (Bretherton et al 2004), the Dynamics and Chemistry of Marine Stratocumulus (DYCOMS) (Stevens et al 2003), and the Variability of the American Monsoon Systems (VAMOS) Ocean-Cloud-Atmosphere-Land Study Regional Experiment (VOCALS-REx) (Jones et al. 2011, Woods et al 2011). These field studies have advanced knowledge of stratocumulus, providing information regarding their boundary layers (MBL), which were under a wide range of aerosol conditions. They have shown that the radiative properties and propensity for drizzle from marine stratocumulus clouds depend on aerosols, liquid water path, and dynamics.

Using data from VOCALS-REx, Jones et al. (2011) found that the boundary layer near the shore of Chile tended to be more shallow, drier, and well mixed compared to the

boundary layer further off the coast, which was deeper, and usually had clouds that produced drizzle. They also found that drizzle and decoupling were correlated, especially heavy drizzle (visibility less than 5/16 of a mile), which only occurred when the boundary layer was decoupled. These findings will be compared to the results of this study to see if these stratocumuli trends are present over the Azores as well. The methods used to differentiate between coupled and decoupled boundary layers in Jones et al. (2011) formed the basis for the methods used in this study to differentiate between coupled and decoupled stratocumuli.

These studies, however, are limited to timescales of only a few weeks to a month. Thus, these studies have not been carried out over a long enough period to provide a useful climatology of key MBL and associated cloud properties. In response to this fact, the U.S. Department of Energy's Atmospheric Radiation Measurement (ARM) Climate Research Facility sponsored a field study for 20 months called the Clouds, Aerosols, and Precipitation in the Marine Boundary Layer (CAP MBL) field campaign, which took place on Graciosa Island in the Azores. Several recent studies have used these data to increase understanding of stratocumulus clouds. Remillard et al. (2012) studied MBL clouds over the Azores using ARM AMF datasets collected during the CAP-MBL field campaign. Cloud occurrence is frequent (60-80%), with a minimum occurring during local summertime (Remillard et al. 2012). Liquid precipitation is frequently present (30-40%), mostly in the form of virga. Boundary layer clouds are the most frequently observed cloud type (40-50%), with occurrences peaking during the summer and fall seasons, when the Azores High is dominant. Cumulus clouds are the most common MBL cloud type (20%) with cumulus under stratocumulus layers (10-30%) and single layer

stratocumulus (0-10%) following in frequency of occurrence. Remillard et al. (2012) also found that a stable transition layer in the subcloud layer is a common feature (present in 92% of all soundings). The transition layer is mainly characterized by a sharp decrease of moisture with height, accompanied by a slight increase in temperature. The presence of this layer is indicative of decoupled conditions that can lead to the upper part of the MBL being cut off from its moisture supply, thus controlling low-level cloudiness. Cumulus cloud bases and stratocumulus cloud tops correlate well with the top of the transition layer and the base of the inversion layer respectively. Remillard et al. (2012) found that stratocumulus clouds over the Azores are almost never coupled to the surface, and that the MBL is almost never well mixed. Another finding from the Remillard et al (2012) study was that drizzling stratocumuli have higher liquid water path (LWP) and cloud thickness values compared with non-drizzling stratocumuli which is consistent with other studies (Wood 2005, Zuidema et al. 2005, Serpetzoglou et al 2008, Kubar et al. 2009).

A complimentary study conducted by Dong et al. (2014a) also used measurements collected at the Azores ARM Mobile Facility (AMF) to produce comprehensive and reliable estimates of seasonal and diurnal variations of marine cloud fraction, MBL cloud macro- and micro- physical properties, and influences of large-scale dynamics. It was found that the high-level and total column cloud fractions were highest during winter, while low-level cloud fraction was greatest during the summer. The higher low-level cloud fraction during the summer was mainly due to the persistent high pressure (Azores High) and dry weather conditions, which are favorable for single-layer MBL clouds. The higher total column and high-level cloud fractions during the winter are mainly due to the frequent low pressure systems and moist air masses, which generate very thick and

multilayered clouds. Mid-level clouds occurred less frequently, and were nearly invariant over the annual cycle. It was also found that the total column and low-level cloud fractions had more pronounced diurnal cycles (higher cloud fractions during the morning and night compared to the afternoon) during the summer than other seasons. Dong et al. (2014a) also found that seasonal variations of cloud heights and thickness are strongly associated with the synoptic pattern seasonal variations. During the summer, cloud top and base heights and cloud thickness values are lower compared to the winter because the summer is dominated by high pressure systems, while the winter is dominated by low pressure systems. During the summer MBL cloud layer LWP and liquid water content (LWC) values are higher than during the winter. The MBL cloud base and top heights along with their corresponding temperatures do not vary significantly diurnally. LWP and LWC do have semidiurnal cycles with larger values at night. The monthly daytime cloud droplet effective radius means are nearly constant while cloud droplet number concentrations follow LWC variations. Cloud droplet number concentrations and cloud condensation nuclei concentrations are strongly correlated from January-May due to dominant low pressure systems that promote upward motions and supply clouds with surface CCN. This correlation is weaker in the summer and autumn months due to the dominance of the Azores High, which promotes sinking motion, not allowing as much surface CCN to reach the cloud layer.

This study focuses on answering several questions about MBL stratocumulus clouds:

1. How often does drizzle occurs under coupled and/or decoupled conditions?
2. How do the macro- and micro-physical properties of stratocumuli change with coupling?

3. Do coupled conditions occur more often during the day or night?
4. How does coupling affect the lifetime of stratocumuli?

The rest of this study is organized as follows. Descriptions of the datasets used in this study are provided in Section 2. Next, the methodology used to select the coupled and decoupled cases in this study and how the statistical properties of the results are calculated are discussed in Section 3. Then in Section 4, the results of this study are shown. Finally, a summary of the results and findings from this study are given in Section 5.

CHAPTER II

DATA

A. Observations

The datasets used in this study were collected with the Atmospheric Radiation Program Mobile Facility (AMF) which was deployed near the north shore of Graciosa Island (39.09° N, 28.03° W, 26 MSL) from May 2009 through December 2010.

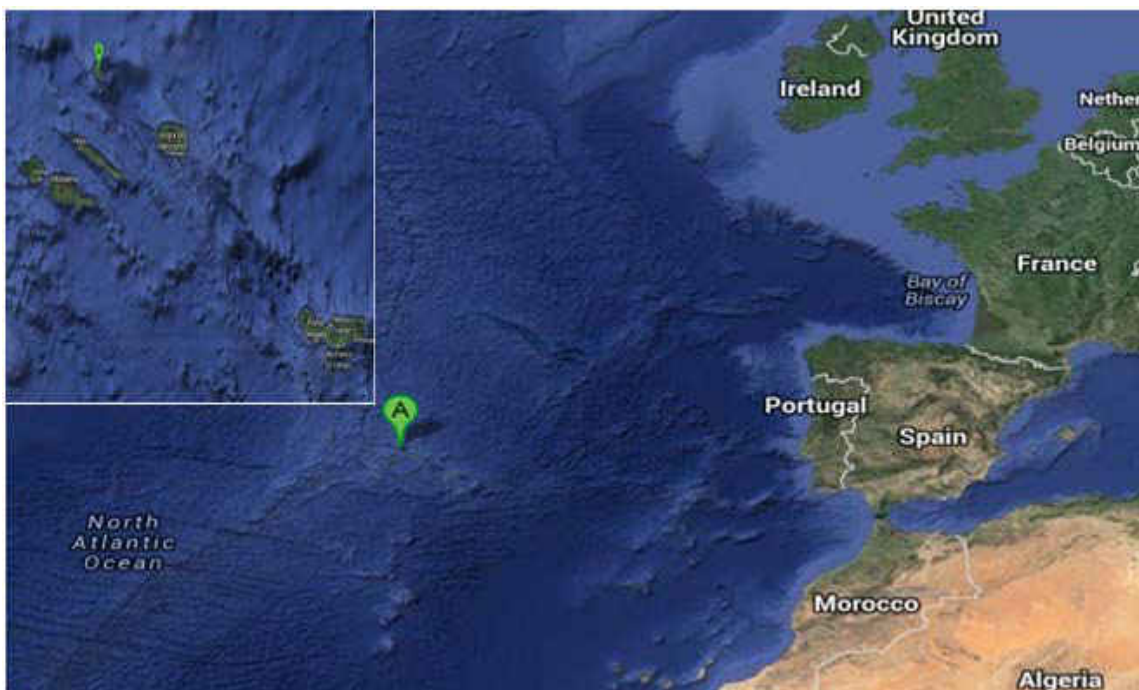


Figure 5. Map showing the location of Graciosa Island with respect to the North Atlantic and Europe. Provided by Google Maps.

This location is upwind for the climatologically prevailing wind conditions in the MBL and was selected to reduce the island effect. One island effect that is reduced by placing it on the north shore is the surface heating because the land surface warms/cools faster than

the ocean surface, resulting in its temperature being higher/lower than over the oceansurface during day/night. The primary instruments used in this study to describe cloud and precipitation conditions include a W-band (95-GHz) Doppler radar, a laser ceilometer, a two channel microwave radiometer, radiosondes, and a micropulse lidar. The instruments were placed within a few meters of each other so that their measurements describe the same atmospheric column. Overall, the observations are fairly continuous with significant overlap between the four remote sensors, both spatially and temporally. Each instrument's time resolution is different from the other, so all data retrieved or collected from each instrument are averaged into five minute intervals. This reduces instrument noise and size, making each data set more manageable. In the next sub-sections, each instrument and retrieval is discussed in greater detail.

1. Microwave Radiometer

The Microwave Radiometer (MWR) is used to measure time-series brightness temperatures at the frequencies of 23.8 GHz and 31.4 GHz, which are sensitive to water vapor and liquid water, respectively. The temporal resolution of the MWR measurements is around 30 s. The brightness temperatures measured with the MWR are then used to retrieve the atmospheric column integrated water vapor (PWV) and liquid water path (LWP) using a statistical method (Liljegren et al 2001). The PWV and LWP retrievals are unreliable during moderate and heavy drizzle events due to contamination of its window (Morris 2006). In this statistical retrieval, the relationships between the opacities and the retrieved PWV and LWP are determined by linear regressions over a large data set, usually made up of radiosonde soundings. The retrieval coefficients are calculated using previous monthly data from the site to account for variations in the underlying parameters

over the course of an annual cycle. The advantages for using this retrieval are that it is simple and reasonably accurate. The disadvantages of this retrieval is that it requires a large prior data set for the specific location which it is applied and it can only be applied at that specific location (Liljegren et al 2001). The root-mean-square (RMS) accuracy of the LWP retrieval is $20 \frac{g}{m^2}$ and 10% for cloud LWP above and below $200 \frac{g}{m^2}$ (Liljegren et al. 2001, Dong et al. 2000).

The MWR was deployed for the whole campaign and it worked continuously without much interruption of data. However, the MWR experienced a processing problem in the second summer, rendering the measurements reported from 11 July through 9 August 2010 unreliable.

2. Balloon Borne Sounding System/ Merged Soundings

The balloon-borne sounding system (SONDE) provides *in situ* measurements (vertical profiles) of both the thermodynamic state of the atmosphere and wind speed and direction. SONDES measure the following parameters as functions of height: Pressure (hPa), Temperature ($^{\circ}\text{C}$), Relative Humidity (RH%), Wind speed (m/s), and Wind direction (degrees). Secondary quantities included in the data stream include: Altitude (gpm), Dew Point ($^{\circ}\text{C}$), Ascent Rate (m/s), Latitude of Sonde ($^{\circ}\text{N}$), Longitude of Sonde ($^{\circ}\text{W}$), u-component of wind velocity (m/s), and v-component of wind velocity (m/s). All of these measurements have a 95.5% confidence level. These radiosondes are launched regularly at 6 hour intervals (Holdridge et al 2011). During the 20-month period of the AMF deployment, more than 2200 atmospheric profiles were collected with sondes, although no sondes were launched in the last third of October 2009 or from 2 December 2009 through 12 January 2010.

The Merged Sounding (MERGESONDE) value-added product (VAP) uses a combination of observations from radiosonde soundings, the microwave radiometer (MWR), surface meteorological instruments, and European Centre for Medium-Range Weather Forecasts (ECMWF) model output with a scaling/interpolation/smoothing scheme in order to produce profiles of the atmospheric thermodynamic state in 1-min temporal intervals for and a total of 266 altitude levels (Table 1 Troyan 2012). Since MERGESONDE data are smoothed and interpolated, some uncertainties can arise from using this product. One error that is seen in some potential temperature profiles is the height of the inversion layer that separates the MBL from the free atmosphere.

Table 1. The vertical resolution for all MERGESONDE altitude levels.

Altitude Range	Resolution
0-3 km AGL	20 m
3-13 km AGL	50 m
13-16 km AGL	100 m
16-20 km AGL	200 m

3. W-Band (95 GHz) ARM Cloud Radar

The W-Band Atmospheric Radiation Measurement (ARM) Program Cloud Radar (WACR) systems are vertically pointing Doppler radars that observe the extent and composition of clouds at 95.04 GHz. Unlike the millimeter wavelength cloud radar (MMCR, 35 GHz), the WACR does not use pulse coding and operates in only copolarization and cross-polarization modes. Millimeter-wavelength radars are ideally

suiting for the study of MBL and high-level clouds owing to its short wavelength (3.15 mm), which is sensitive enough to detect cloud droplets (-50 dBZ at 2 km), while only slightly attenuating when light to moderate drizzle is present. The WACR also provides high temporal and spatial resolutions (around 2 s and 43 m) because it uses a narrow beamwidth (0.19°). The WACR can also provide accurate estimations of cloud base and cloud top heights. The WACR, however, does attenuate when heavy precipitation is present, and is therefore unreliable in depicting thick precipitating clouds (Widener and Johnson 2006).

For the Azores deployment, the WACR began operating on the morning of 5 June 2009 and was operated to the end of December 2010. One major interruption occurred in September 2010, when the radar was down for 23 days, due to a hard disk problem. Other than that, the radar also experienced six downtimes of more than an hour (including three that extended for more than 1.5 days.) and a few shorter, for a total of less than 10% of a month.

4. Aerosol Observing System

The Aerosol Observing System (AOS) is a suite of in situ surface measurements of aerosol optical and cloud-forming properties. The instruments measure aerosol properties that influence the Earth's radiative balance. The primary optical measurements are those of the aerosol scattering and absorption coefficients as a function of particle size and radiation wavelength, and of cloud condensation nuclei concentration (CCN) measurements as a function of percent super-saturation. Some uncertainties with the dataset include: instrument noise in the filtered air scattering coefficient, instrument calibration drift, uncertainty in the instrument calibration due to Rayleigh scattering of

dry air and CO_2 , instrument truncation of near forward scattered light, and the uncertainty in the instrument pressure and temperature in conversion of the data to STP (Jefferson 2011).

The AOS was operational for the whole campaign. It did, however, experience a period (1 Jan 2010 – 2 June 2010) where there was a slow decline in the CCN signal. This decline in the CCN signals makes all CCN observations in this time period unreliable. The reason for this decline is unknown as all the instruments operating parameters appeared normal. The decline was likely from a change in the CCN column thermal properties or clogging of the detector inlet.

5. Vaisala Ceilometer

The Vaisala Ceilometer (VCEIL) is a self-contained, ground-based, active, remote sensing device designed to measure cloud-base height and vertical visibility. It detects up to three cloud layers simultaneously, but only the bottom cloud layer observations are usually reliable due to the loss of lidar signal owing to cloud droplets. It has a maximum vertical range of 7700 m. It has a vertical resolution of 15 m (Morris 2012). The VCEIL is more accurate at depicting the cloud base height than the WACR, and is more accurate than the micropulse lidar (MPL) during heavy precipitation because MPL signals are attenuated.

Similar to other instruments, the VCEIL also provided nearly continuous measurements during the whole campaign. It only experienced 12 downtimes lasting more than an hour (including three covering more than a day) as well as a small number of shorter interruptions.

6. NASA LARC Satellite Products (Meteosat-9)

The European geostationary satellite Meteosat-9 provides images of the Azores every hour. The MSG satellite carries a pair of instruments called the Spinning Enhanced Visible and InfraRed Imager (SEVIRI) and the Geostationary Earth Radiation Budget (GERB) instrument. The SEVIRI observes the Earth in 12 spectral channels, while the GERB can be used for Earth radiation budget studies because it is a visible infrared radiometer.

- B. Retrieved MBL cloud microphysical properties from the ARM AMF dataset
1. Cloud droplet effective radius (re)

The daytime MBL cloud droplet effective radius was calculated using (Dong et al, 1998)

$$re = 2.07 + 2.49LWP + 10.25\gamma - .25\mu_0 + 20.28LWP\gamma - 3.14LWP\mu_0, \quad (1)$$

where re is cloud droplet effective radius, LWP is liquid water path, γ is the ratio between measured cloud sky and inferred clear-sky downward solar fluxes at the surface, and μ_0 is the cosine of the solar zenith angle. The uncertainties of re daytime retrievals are approximately 10%. For nighttime hours, the equation in (Dong et al. 2014b) was used to calculate the profiles of cloud droplet effective radius

$$re(h) = \frac{\exp(3.912 - .5\sigma_x^2)}{N^{.167}} \exp(0.0384dBZ(h)) = a \exp(0.0384dBZ(h)) \quad (2)$$

where N is the cloud droplet number concentration, $dBZ(h)$ is the radar reflectivity at a certain height h , σ_x is the logarithmic width, and the coefficient a is either 22.7 from November to February, and 26.78 for the rest of the months. The uncertainty for nighttime re retrievals is approximately 20% (Dong and Mace 2003).

2. Cloud droplet number concentration (N_d)

The cloud droplet number concentration N_d was also calculated from Dong et al. (2014b) using,

$$N_d = LWC / [(4)\pi\rho_w r_e^3 \Delta Z] \exp(-3\sigma_x^2), \quad (3)$$

where r_e is the cloud droplet effective radius, ρ_w is the density of water, σ_x is logarithmic width, ΔZ is cloud thickness, and LWC is the liquid water content. The daytime uncertainty of N_d retrievals is between 20%-30%. Nighttime retrieval of N_d are obtained using (2) as well, with an uncertainty between 30%-40%. Table 2 lists the cloud parameters, and their corresponding instruments/methods and uncertainties used in this study.

Table 2. Uncertainties of instruments/methods used in this study.

Cloud Parameter	Instrument/Method	Uncertainty	Reference
Cloud Base Height	Ceilometer	15 m	Remillard et al. (2012)
Cloud Top Height	W-Band Radar	43 m	Remillard et al. (2012)
Cloud Base/Top temperature	Merged Sounding	0.2 °C	ARM Website
LWP	Microwave Radiometer	~20 $\frac{g}{m^2}$ for LWP < 200 $\frac{g}{m^2}$ and 10% for LWP > 200 $\frac{g}{m^2}$	Dong et al. 2000 Liljegren et al. (2001)
LWC	LWP/Cloud Thickness		
r_e	Dong et al. 1998 and Dong et al. 2014b parameterizations	10% daytime 20% nighttime	Dong et al. (1998, 2014b)
N_d	Dong et al. 1998 and Dong et al. 2014b parameterizations	20-30% daytime 30-40% nighttime	Dong et al. (1998, 2014b)
NCCN	AMF Aerosol Observing System		ARM Website

CHAPTER III

METHODOLOGY

A. Case selection

The first step of selecting cases for this study was choosing days that had persistent clouds (lasting more than 2 hours) whose cloud top heights were less than 3 km (Dong et al. 2014a). Once this was done, two methods (Potential Temperature and Lifting Condensation Level LCL) were used to choose days with distinct coupled and decoupled periods. Then, satellite images from Meteosat-9, along with WACR reflectivity profiles were used to identify stratocumulus clouds. Finally, results from the chosen days were classified into three different sub-groups: coupled vs. decoupled, non-drizzling vs. drizzling, and day vs. night. In this section, case selection using both the potential temperature and LCL methods is described. The seven coupled or decoupled cases have been identified by both methods in this study.

1. Potential Temperature Method

One way to differentiate between coupled and decoupled stratocumulus clouds is to analyze the vertical potential temperature profile. For a cloud layer to be coupled with the surface, the boundary layer below the cloud layer must be well mixed. This means that turbulence is strong enough to mix the boundary layer so that properties such as mixing ratio are uniform vertically. As demonstrated in Fig. 6b, the potential temperature is nearly constant from the surface to the stratocumulus cloud base for a well-mixed

boundary layer, while for the decoupled case, the potential temperature is not constant with height (Fig 6a).

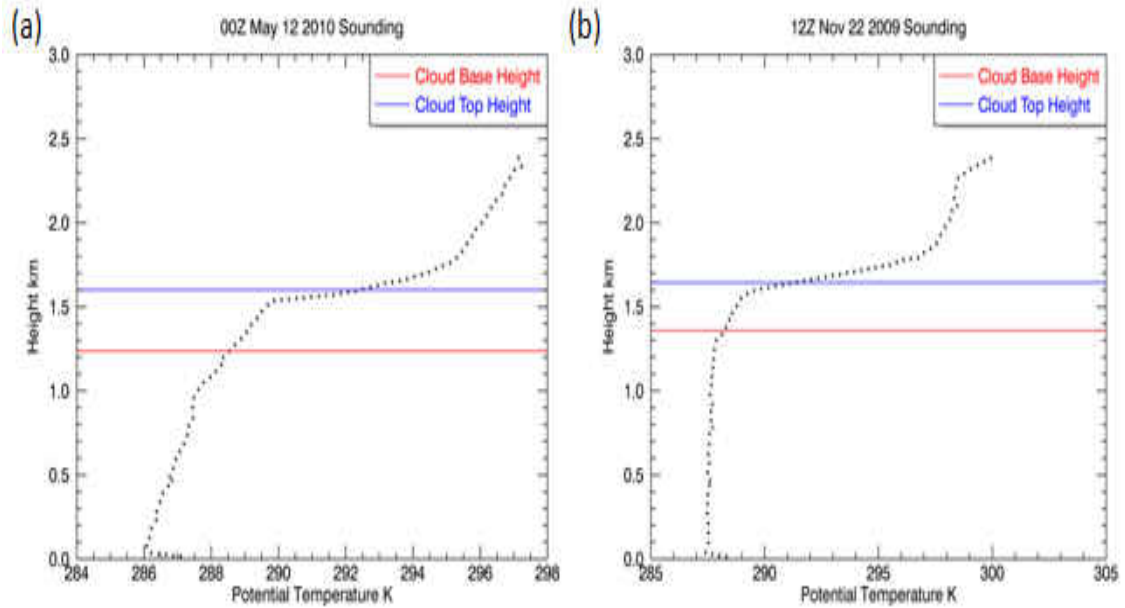


Figure 6. Potential temperature profiles for a well mixed boundary layer (b) and a decoupled boundary layer (a).

Before the potential method can be used, the sub-cloud layer must be defined. The cloud base height is used to define the top of the sub-cloud layer, which is derived from the ceilometer instrument. The bottom of the sub-cloud layer is defined as the top of the surface layer, which is approximately 300 meters above ground level (AGL). The surface layer is not included in the sub-cloud layer in this study, because it is heavily influenced by surface heating/cooling fluxes. The sounding data used in this study were taken over land, which cannot be used to represent the actual surface heating/cooling fluxes over the ocean. Over land, the surface warms/cooling more quickly than the ocean, which can lead to false signals in the vertical potential temperature profile relative to conditions over water, such as inversion layers at night. Once the sub-cloud layer is defined, the potential temperature profile of this layer can be defined as either well mixed or decoupled using

$$|\theta_{top} - \theta_{bot}| < 0.5 \text{ K}, \quad (4)$$

$$|\theta_{lvl} - \theta_{lvl-1}| < 0.5 \text{ K}, \quad (5)$$

$$|\theta_{lvl} - \theta_{top}| < 0.5 \text{ K}, \text{ and} \quad (6)$$

$$|\theta_{lvl} - \theta_{bot}| < 0.5 \text{ K}, \quad (7)$$

where θ_{top} is the averaged potential temperature of the top 25% of the sub-cloud layer, θ_{bot} is the averaged potential temperature of the bottom 25% of the sub-cloud layer, and θ_{lvl} is the potential temperature at a certain height (AGL) between the top and bottom of the sub-cloud layer. The potential temperatures for the top and bottom of the sub-cloud layer are averaged to prevent a bad data point from producing an incorrect classification of a layer as decoupled. The threshold 0.5 K used in (4-7) is suggested by Jones et al. (2011) and seems arbitrary, but does enable accurate differentiation between coupled and decoupled boundary layer. If the difference between the averaged potential temperatures for the bottom and top of the sub-cloud layer is greater than 0.5 K, then the sub-cloud layer is considered to be decoupled. If the temperature difference in (4) is less than 0.5 K, then (5-7) are used to evaluate whether the potential temperature is constant within the middle of the sub-cloud layer. At first, the potential temperature at the selected height level is compared to the potential temperature immediately below it, and then the potential temperature of the current level is compared to the potential temperatures at the top and bottom of the sub-cloud layer. If 90% of the potential temperature differences at the height levels between the top and bottom of the sub-cloud layer are less than 0.5 K and differences between the top and bottom of the sub-cloud layer are less than 0.5 K, then the sub-cloud layer is considered to be well-mixed, and therefore the surface is coupled to the cloud layer.

In addition to using the potential temperature profile, the water vapor mixing ratio profile are also be used to determine if the boundary layer is well-mixed. The equation used to calculate water vapor mixing ratio is

$$w = \frac{R' e}{R_v p}, \quad (8)$$

where w is the water vapor mixing ratio, R' is the dry air gas constant ($287 \frac{J}{kg K}$), R_v is the water vapor gas constant ($461.5 \frac{J}{kg K}$), e is the water vapor pressure, and p is the air pressure. Using (4-7) with mixing ratios and 0.5 g/kg as the threshold between well-mixed and decoupled instead, the sub-cloud layer can be defined as well-mixed or decoupled from the surface.

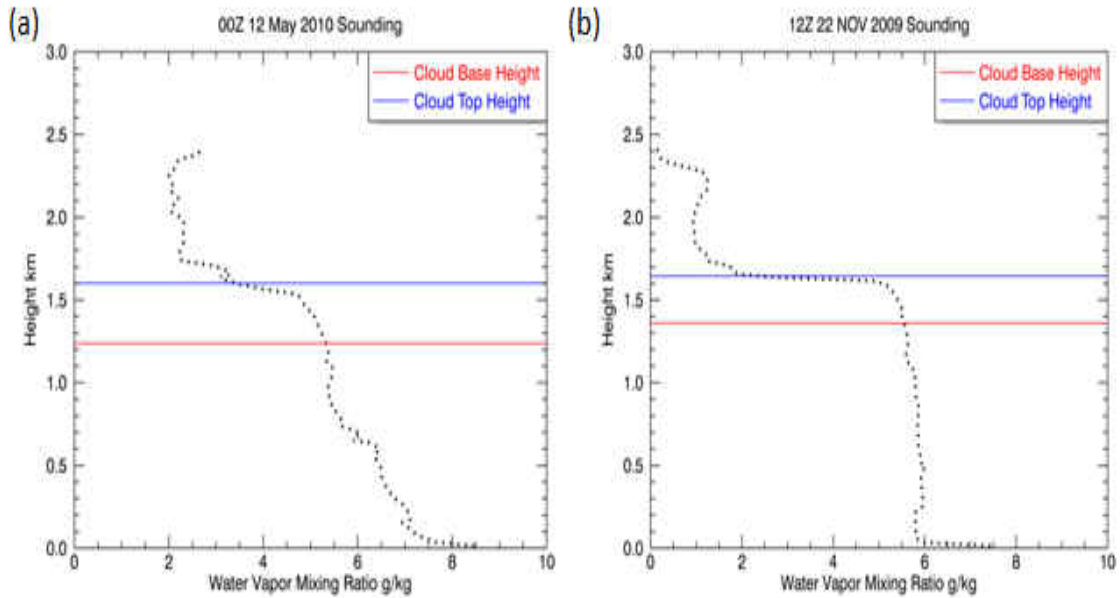


Figure 7. Water vapor mixing ratio profiles for a well mixed boundary layer (b) and a decoupled boundary layer (a).

As shown in Fig. 7b, the coupled case had a near constant water vapor mixing ratio from the surface to the base of the inversion layer at the cloud top. For the decoupled case (Fig. 7a), the mixing ratio was not constant within the boundary layer; instead it decreased steadily with height.

1a. Comparison of Potential Temperature Method to Similar Methods

Other researchers (Remillard et al. 2012, Jones et al. 2011) have used the vertical liquid potential temperature profile for the whole boundary layer to determine whether a cloud layer is coupled or decoupled from the surface. The methods used by Remillard et al. (2012) and Jones et al. (2011) investigate whether the whole cloud layer is coupled to the surface. Clouds over the Azores, however, are rarely fully coupled to the surface because of cloud-top entrainment (Remillard et al. 2012). Thus, only the vertical potential profile below the cloud layer is used to define whether a cloud layer is coupled or decoupled from the surface in this study. Although this method does account for the effect of surface fluxes on the lower part of the cloud layer, it cannot determine if cloud-top entrainment is occurring. Another difference between the method used in Jones et al. (2011) and that used herein is that this method uses the potential temperature values for the whole layer, rather than only using the top 25% and bottom 25% of the potential temperature values. This ensures that the whole layer is well mixed.

2. Lifting Condensation Level (LCL) Method

In this method, both the LCL and cloud base heights are used to determine whether a cloud layer is coupled or decoupled from the surface. For a well-mixed boundary layer, the LCL and cloud base heights will be approximately the same. As the degree of decoupling increases, the LCL and cloud base heights will diverge (Jones et al. 2011). To calculate the LCL height, the Espy equation is used,

$$h_{lcl} = 125(T - T_d) \quad (9)$$

where 125 is the inverse difference between the dry adiabatic lapse rate ($9.8 \frac{K}{km}$) and the dew point lapse rate ($1.8 \frac{K}{km}$), T is the temperature at the surface, and T_d is the dew point

temperature at the surface. Once the LCL height is calculated, the difference between it and the cloud base is calculated using

$$\Delta z = |z_b - z_{LCL}|, \quad (10)$$

where z_b is the cloud base height and z_{LCL} is the LCL height. If this difference is less than 150 m then the boundary layer is considered to be well mixed (Jones et al 2011).

3. Comparison between LCL and Potential Temperature Methods

For the selected cases, both methods agree reasonably well, with the potential temperature method classifying 28% of the MBL clouds as coupled to the surface, while the LCL method classified 39% of MBL clouds as coupled to the surface. This is consistent with Jones et al. (2011), who found the MBL off the western coast of South America to be well mixed 28% of the time using an empirical decoupling threshold for cross MBL differences in total water mixing ratio and liquid potential temperature and 45% of the time using a method similar to the LCL method.

4. Drizzle vs Non-Drizzle

Besides comparing coupled and decoupled stratocumulus layers, this study also compares drizzling and non-drizzling stratocumuli for the following two reasons: (1) drizzle is a strong indicator that the stratocumulus layer is decoupling (Wood 2004), and (2) drizzle regulates the magnitude of key cloud microphysical properties such as LWP, r_e , N_{CCN} , and N_d . To differentiate between drizzling and non-drizzling clouds, W-Band cloud radar and VCEIL data were used. If there were radar reflectivity values greater than -60 dBZ below the ceilometer derived cloud base height, then the cloud is considered to be drizzling. Although the cloud may be drizzling below the cloud base, this method does not differentiate between virga and drizzle reaching the ground.

. The Two Sample Student T-Test was used to test the statistical significance of the differences between coupled and decoupled mean values for different cloud parameters at a confidence level of $\alpha=0.5$. The equation for the two sample T-Test is,

$$\dots\dots\dots t = \frac{\bar{x}_1 - \bar{x}_2}{\sqrt{\frac{s_1^2}{n_1} + \frac{s_2^2}{n_2}}}, \dots\dots\dots (11)$$

where t is the T-value, s is the standard deviation, n is the sample size, and \bar{x} is the sample mean. A normal distribution with independent samples and two independent populations are necessary to carry out this test. Decoupled and coupled stratocumulus clouds are considered to be independent of each other, and most cloud parameter distributions are close to a normal distribution to use this test. The T-Test, however, cannot be used for the coupled cloud height distribution, because it is bimodal and is therefore not shown in this study. The samples used in this study are not independent of each other, due to their time dependence on each other. This leads to an underestimation of the variance of the samples, which will decrease the accuracy of the T-Test.

Autocorrelation decreases the sample size, which increases the magnitude of the denominator in the T-Test, thus compensating for the underestimated variance. The equation used to calculate the autocorrelation coefficient is,

$$\rho_x(L) = \frac{\sum_{k=0}^{N-L-1} (x_k - \bar{x})(x_{k+L} - \bar{x})}{\sum_{k=0}^{N-1} (x_k - \bar{x})^2}, \quad (12)$$

where x is a sample value, L is the set lag which is set at 1 for this study, N is the total number of samples, and \bar{x} is the sample mean. The new sample size n' is calculated using,

$$n' = n \frac{1-\rho}{1+\rho}, \quad (13)$$

where ρ is the autocorrelation coefficient and n is the sample size.

The other test that was used to examine the significance of the difference of means between the selected cloud parameters was the effective size. This test measures the actual significance of a statistical result. This is a necessary test for any statistical results, because a statistical result can be statistically significant, but not have practical significance. There are multiple ways to measure effective size, but this study will only use the Cohen's d value, which is given by

$$\frac{\bar{x}_1 - \bar{x}_2}{s_{pooled}}, \quad (14)$$

where \bar{x} is the sample mean and s_{pooled} is the pooled standard deviation for both samples. The significance levels for Cohen's d values are as follows: $d < 0.2$ no effect, $0.2 < d < 0.5$ small effect, $0.4 < d < 0.8$ intermediate effect, and $d > 0.8$ strong effect (Cohen 1988).

CHAPTER IV

Results/Discussion

A. Cases Selected

Using the methodologies described in the previous section, seven cases (2-3 days in length each) were chosen with five having coupled periods and two having no coupled periods, during the 19-month period. Except for one that occurred in the late spring all selected cases occurred in the autumn. This is consistent with Dong et al. (2014a) and Remillard et al. (2012) where they found that MBL clouds occurred most frequently during the summer and fall when the Azores High is dominant. Below is a list of the cases chosen.

Table 3. List of cases chosen.

List of Cases
10/21/09-10/22/09
11/02/09-11/03/09
11/22/09-11/23/09
05/11/10-05/12/10
10/02/10-10/04/10
10/11/10-10/12/10
11/07/10-11/09/10

For the selected cases, both the LCL and the potential temperature methods were applied and the results agreed well with each other. The LCL method did, however, overestimate the length of the coupled period on 21 October, 2009, which is consistent with the findings of Jones et al. (2011). The LCL method also did not catch the coupled periods on 12 October, 2010 and 8 November, 2010, presumably due to the use of the dew point temperature and air temperature at 300 m to calculate the LCL height in the LCL method. This can sometimes lead to the LCL height being lower than it is in reality, thus making the difference between the LCL and cloud base height greater than 150m and classifying the samples as decoupled. Out of these seven cases, a total of 2562 5-min samples were used to compute the statistical characteristics. Out of the 2562 total samples, 726 samples (28.3%) were classified as coupled, 1836 (71.7%) as decoupled; 1766 (68.9%) as drizzle, 796 (31.1%) as non-drizzle; 872 (34%) as day, and 1690 (66%) as night. Thirty-seven percent of the coupled samples are also non-drizzling, while only 29% of the classified decoupled samples are non-drizzling. Thus the decoupled samples have a higher frequency of drizzling events compared to the coupled samples. Of all the classified daytime samples (872), 67% were also drizzling samples. Of all the classified nighttime samples (1766), 70% were also drizzling samples. Thus drizzling events are dominant for both daytime and nighttime. For the selected 726 coupled cases, they include 160 (18%) daytime samples and 566 (34%) nighttime samples, indicating there are more coupled events during the nighttime than during the daytime.

B. MBL cloud properties

For the 22-23 November, 2009 case, the stratocumulus layer was coupled for most of the period (0-32 UTC). As illustrated in Fig. 9a, the radar reflectivity clearly

showed the mesoscale structure of the stratocumulus layer oscillating between updrafts (low reflectivity) and downdrafts (high reflectivity) every 2-3 hours, which is consistent with the findings of Miller et al. (1995). Virga, which is drizzle that does not reach the surface, was present for most of the case. The cloud top/base heights for the period were relatively constant (1.6 km, 1.3 km respectively), which made the cloud thickness relatively constant (300 m) throughout the period (Fig. 9b). High/low values of LWP coincided with high/low radar reflectivity and down/updrafts (Fig. 9c). For this case, most LWP values remained below $150 \frac{g}{m^2}$ due to the lack of heavy precipitation. The r_e values followed the variation of LWP, with small values coinciding with updraft regimes due to condensational growth and large values coinciding with downdraft regimes due to the collision and coalescence processes (Fig. 9d). N_d values, however, showed a negative correlation with LWP and r_e values meaning that low N_d values corresponded with high LWP and r_e values, while high N_d values corresponded with small LWP and r_e values. Most N_d values were below $300 \frac{\#}{m^3}$ (Fig. 9e), and dropped below $100 \frac{\#}{m^3}$ for drizzle events due to the collision and coalescence of cloud droplets by drizzle droplets. N_{CCN} values remained relatively constant around $400 \frac{\#}{m^3}$ throughout the case (Fig. 9e).

To further investigate their vertical distributions, cloud temperature, LWC, and r_e profiles were normalized from the cloud base (0) to the cloud top (1) through the entire case. As shown in Fig 10a, cloud temperature decreased from 277.5 K at the cloud base to 276.5 K just above the center of the cloud and then sharply increased to ~ 279 K at the cloud top. This strong inversion layer is the primary factor in maintaining a constant and thin cloud layer (~ 300 m) throughout the period. Both the r_e and LWC profiles were

nearly constant for the bottom half of the cloud, and then decreased for the top half of the cloud (Figs. 10b, 10c) due to cloud top entrainment.

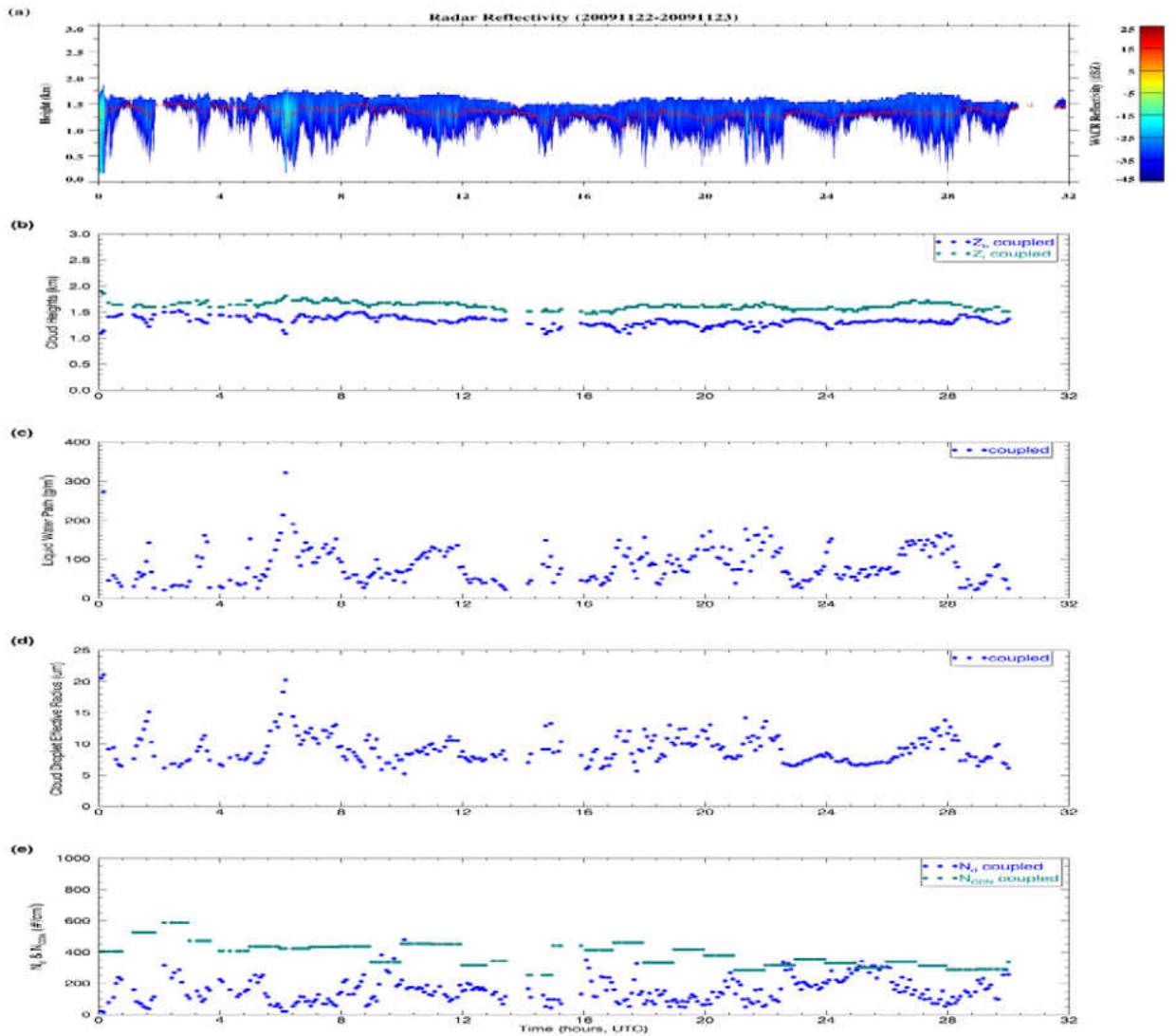


Figure 9. Time series of (a) radar reflectivity, (b) cloud-base (Z_b) and -top (Z_t) heights derived from ARM radar-lidar measurements, (c) cloud liquid water path (LWP) retrieved from microwave radiometer, (d) cloud-droplet effective radius (r_e) (e) cloud droplet number concentration (N_d) and cloud condensation nuclei concentration (N_{CCN}) coupled and decoupled conditions during the 22-23 November, 2009 case.

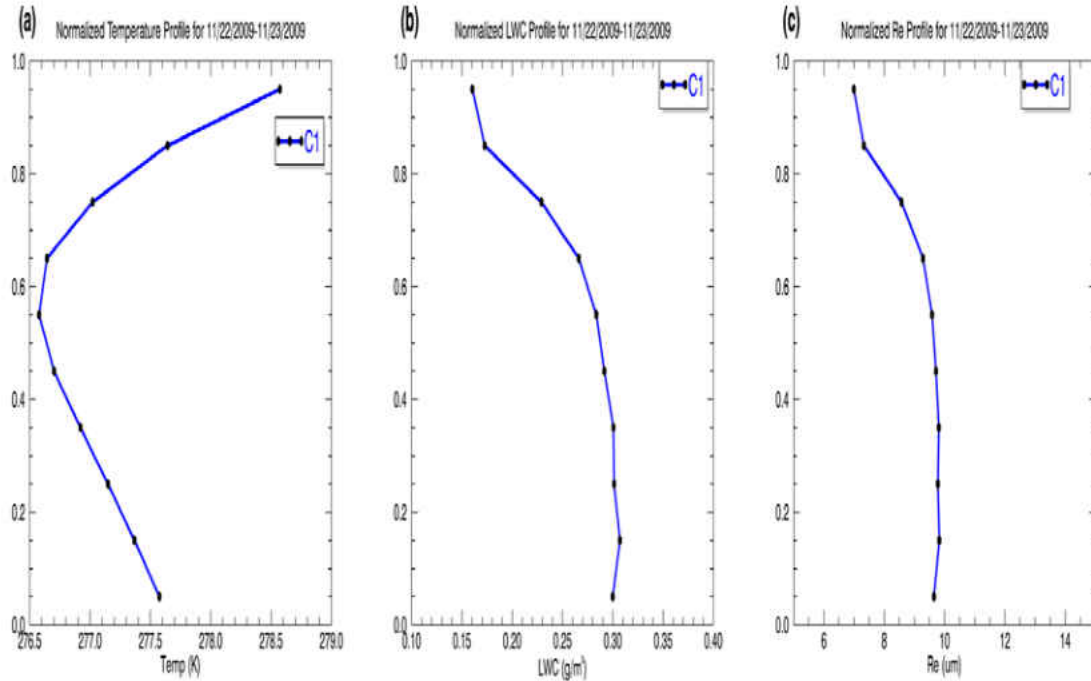


Figure 10. Normalized profiles of (a) temperature, (b) LWC, and (c) r_e for the 22-23 November, 2009 case.

The case of 11-12 May, 2010 case was decoupled for the whole period (Fig. 11). The radar reflectivity shows a mesoscale structure that has similar characteristics as the coupled case, but also has significant differences, such as several periods with drizzle reaching the surface, and a few broken periods. As illustrated in Fig. 12, the hourly satellite images clearly show the open cells of the MBL cloud layer during radar-reflectivity-indicated broken periods, such as 15-18 UTC 11 May and 13-19 UTC. This is in contrast with the previous coupled case, where the cloud layer was unbroken and had few heavy drizzle events. The cloud top/base heights fluctuated frequently during this case, with clouds thickening during heavy drizzle periods and thinning when drizzle was not present (Fig. 11b). Maximum cloud top/bases heights were 2.5 km and 2 km respectively, and had minimums at 1 km and 0.75 km respectively. This is in contrast with the coupled case, where the cloud heights did not fluctuate frequently due to do lack

of heavy drizzle events. LWP values also fluctuated frequently with values greater than $150 \frac{g}{m^2}$ when heavy drizzle occurred (Fig. 11c). The r_e values also followed the same variations of LWP values, with larger r_e values during the precipitation periods than those without drizzle occurring. It is clearly shown that both LWP and r_e values in this case are larger than those in the coupled case in Fig. 9. In contrast, the N_d and N_{CCN} values are lower than those in Fig. 9. Most of the N_d values were below $100 \frac{\#}{m^3}$, dropping significantly when heavy drizzle was present. N_{CCN} values were also significantly lower for this case, with most of the N_{CCN} values being below $50 \frac{\#}{m^3}$ (Fig. 11e). Since N_d exceeded N_{CCN} for most of the period, the surface was not the primary source of cloud nuclei for the cloud layer. Using the back-trajectory method to track the air mass source, it was found that the air mass was primarily advected from north of the Azores which had no strong evidence of pollution.

The normalized temperature profile for this case also shows an inversion layer present within the cloud, which is similar to the coupled case. The inversion layer in this case, however, was located in the upper 80% of the cloud layer (Fig. 13a), while the coupled case had the inversion layer located in the upper 60% of the cloud layer (Fig. 10a). Also, the temperature inversion strength was around $\Delta T=0.5$ K, which was much weaker than the coupled case ($\Delta T>2$ K). Due to the higher location of the inversion layer in this case, the cloud layer had a greater opportunity to thicken compared to the coupled case. The normalized LWC and r_e profiles for this case are both relatively constant at the bottom of the cloud layer, and begin to decrease at the upper part of the cloud layer. This trend is similar to the coupled case, but this case has higher LWC and r_e values due to the greater amount of drizzle.

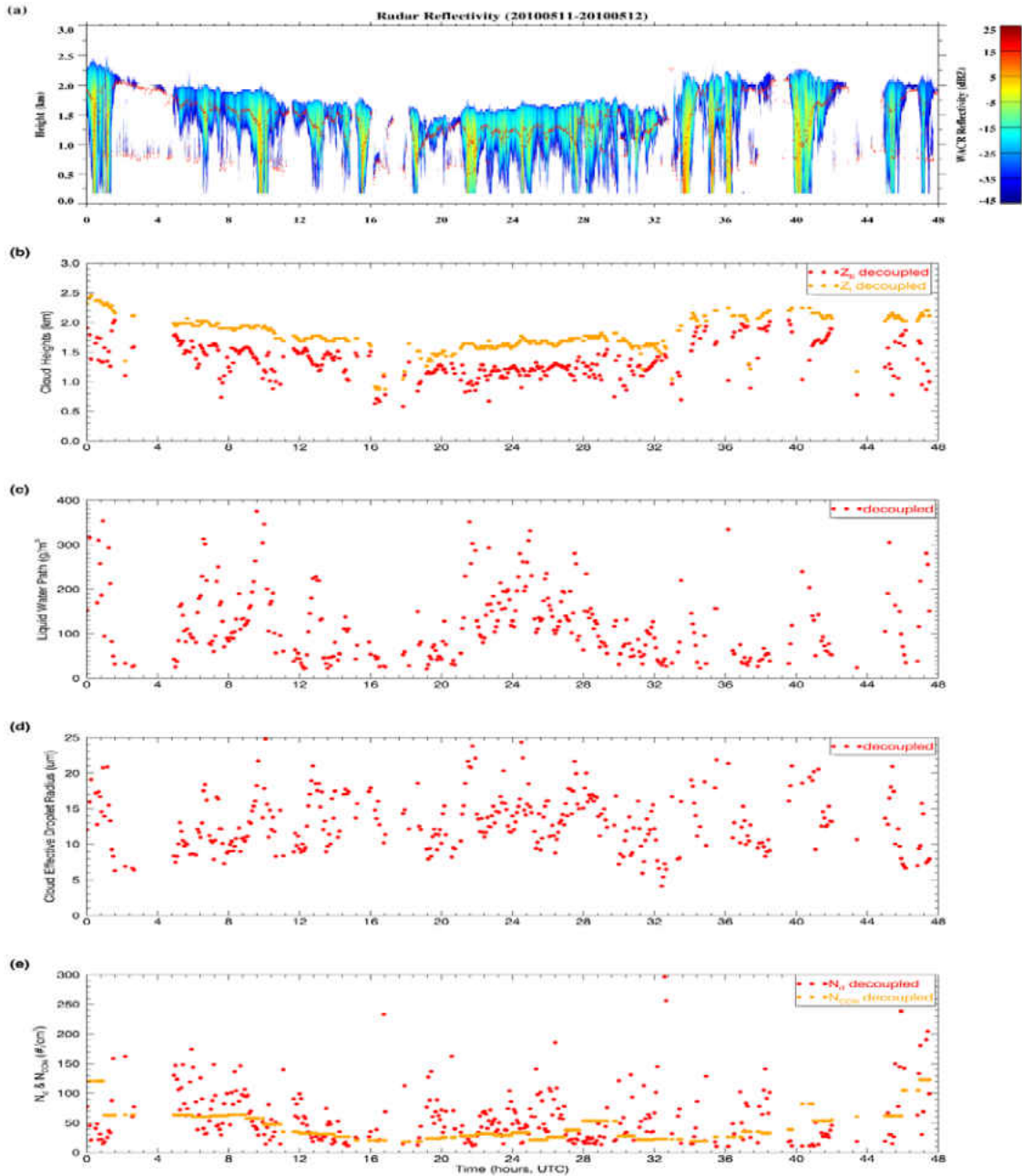


Figure 11. Time series of (a) radar reflectivity, (b) cloud-base (Z_b) and -top (Z_t) heights derived from ARM radar-lidar measurements, (c) cloud liquid water path (LWP) retrieved from microwave radiometer, (d) cloud-droplet effective radius (r_e), and (e) cloud droplet number concentration (N_d) and cloud condensation nuclei concentration (N_{CCN}) under coupled and decoupled conditions during the 11-12 May, 2010 case.

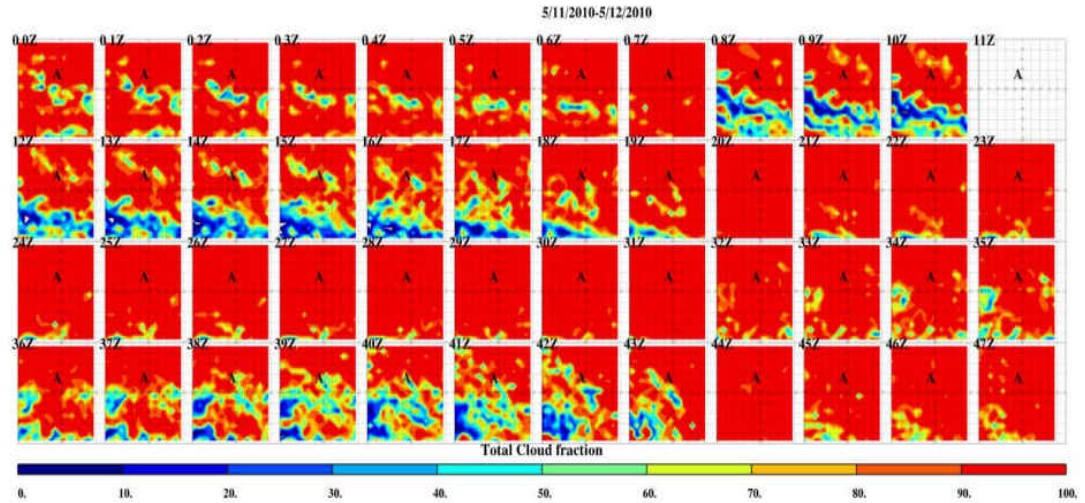


Figure 12. As in Fig. 11, but for hourly satellite images within a grid box of $.5^{\circ} \times .5^{\circ}$ centered on the ARM Azores site (with symbol A).

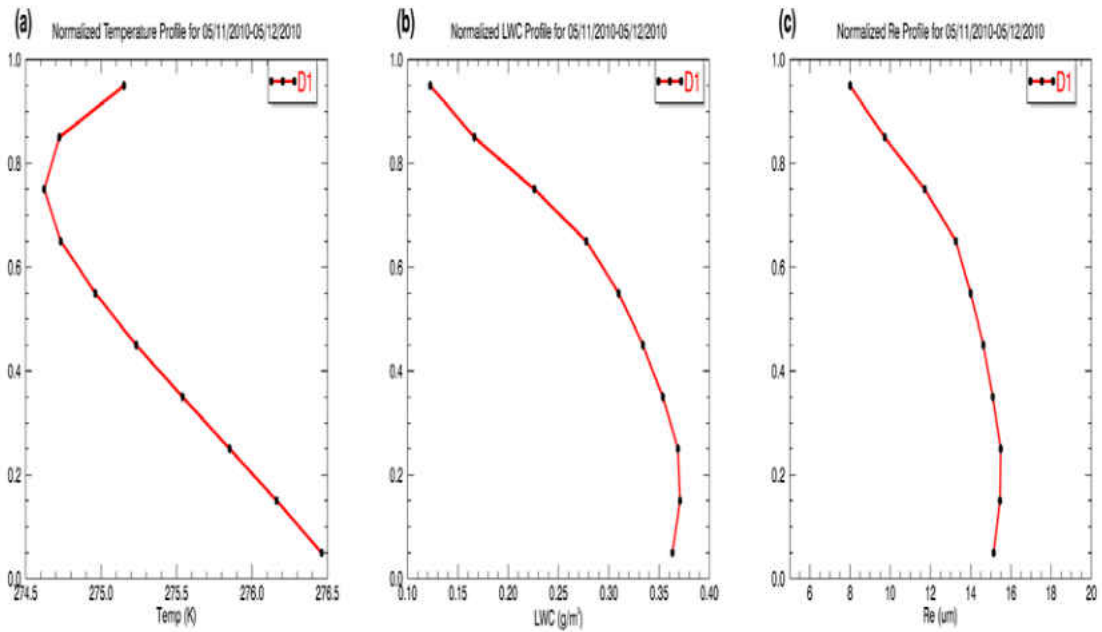


Figure 13. Normalized profiles of (a) temperature, (b) LWC, and (c) r_e , for the 11-12 May, 2010 case.

For the 2-4 October 2-4, 2010, case the stratocumulus cloud layer was decoupled from the surface for the whole period. As shown in Fig. 14a, the cloud layer was initially thick with heavy drizzle present, thinned significantly during the period of 28-42 UTC,

and thickened again during the period of 43-47 UTC. Fig. 14b shows that, except for several long breaks, the cloud layer over the Azores remained a solid and overcast layer for most of the period. Cloud heights fluctuated significantly throughout the case with higher (lower) cloud tops (bases) coinciding with heavy drizzle events. This is consistent with the previous decoupled case, which also had fluctuating cloud heights, due to drizzle events. As shown in Fig. 14c, the LWP values initially were greater than $200 \frac{g}{m^2}$ due to heavy drizzle and then sharply dropped for the rest of period except for the final hours due to thinning of the cloud layer and absence of drizzle. Again the r_e values followed the variations of LWP, with higher r_e values occurring during heavy drizzle (Fig. 14d). Fig. 14e shows that N_d values fluctuated frequently throughout the period, with concentrations greater than 200 cm^{-3} during non-drizzle periods and concentrations less than 100 cm^{-3} during drizzle. The N_{CCN} values remained between 400 and 600 cm^{-3} for the first half of the event, and then decreased for the latter half of the case until 56UTC, when it increased towards the end of the case (Fig. 14e).

As illustrated in Fig. 15a, the normalized temperature profile shows that there was an inversion layer present in the upper part of the cloud layer. Compared to the coupled and decoupled cases, the inversion layer in this case is higher than the coupled case, but lower than the other decoupled case. The inversion strength ($\Delta T \sim 1\text{K}$) for this case is weaker than the coupled case ($\sim 2\text{K}$) but stronger than the other decoupled case ($\sim 0.5\text{K}$). Similar to both the coupled and decoupled cases, LWC in Fig. 15b is relatively constant for the bottom half of the cloud layer, but steadily decreases for the upper half of the cloud. The maximum LWC value for this case is lower than those from both the coupled and decoupled cases because for more than half the case, the cloud layer was

very thin. In Fig. 15c, the normalized r_e profile has characteristics that are similar to those of the LWC profile. The maximum r_e values are slightly larger than those from the coupled case due to the increased amount of heavy drizzle events in the decoupled case. The maximum r_e values for this case were lower than those from the other decoupled case, because the other decoupled case had more heavy drizzle events.

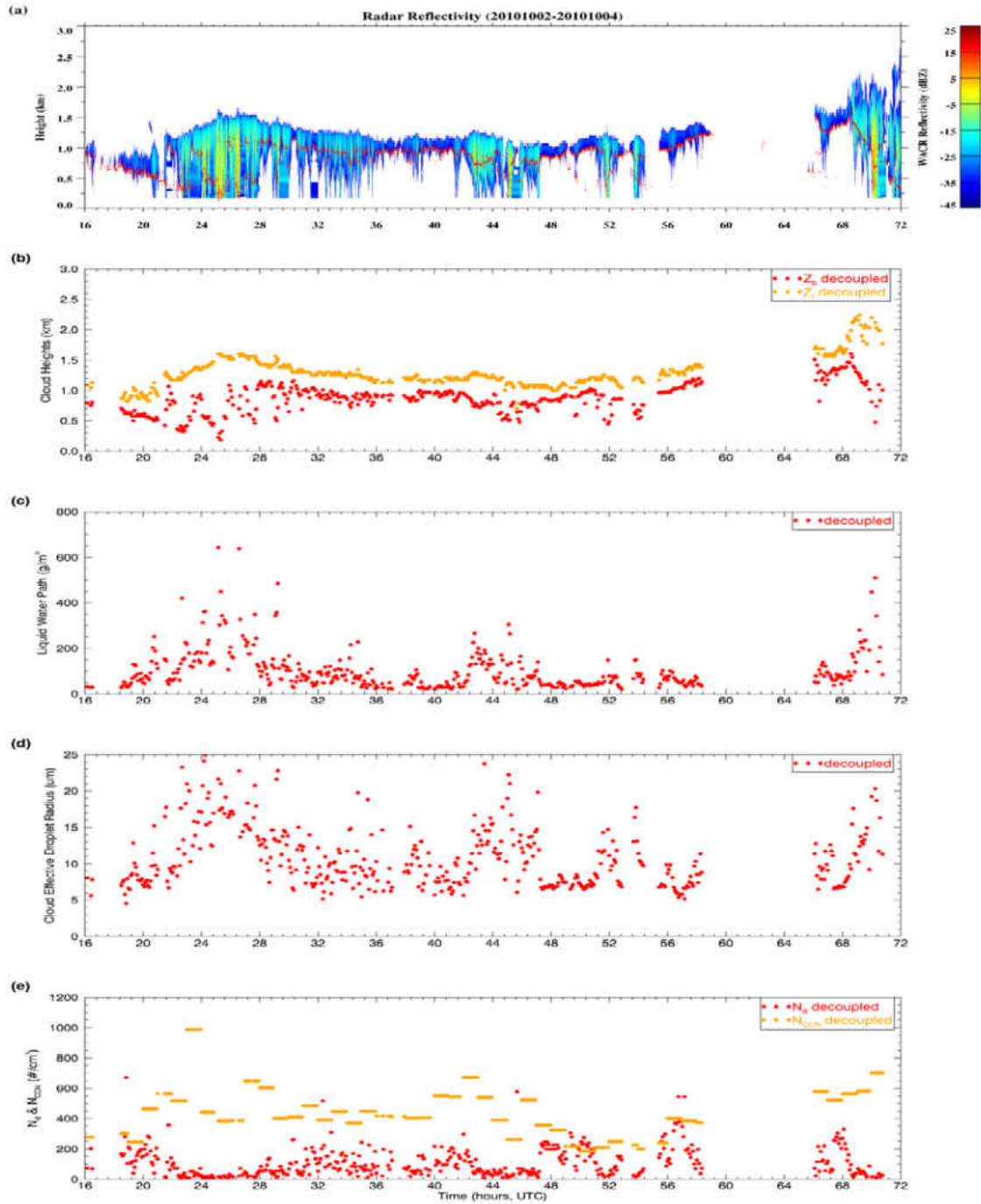


Figure 14. Time series of (a) radar reflectivity, (b) cloud-base (Z_b) and -top (Z_t) heights derived from ARM radar-lidar measurements, (c) cloud liquid water path (LWP) retrieved from microwave radiometer, (d) cloud-droplet effective radius (r_e), and (e) cloud droplet number concentration (N_d) and cloud condensation nuclei concentration (N_{CCN}) under conditions of coupled and decoupled during the period, 2-4 October, 2010 case.

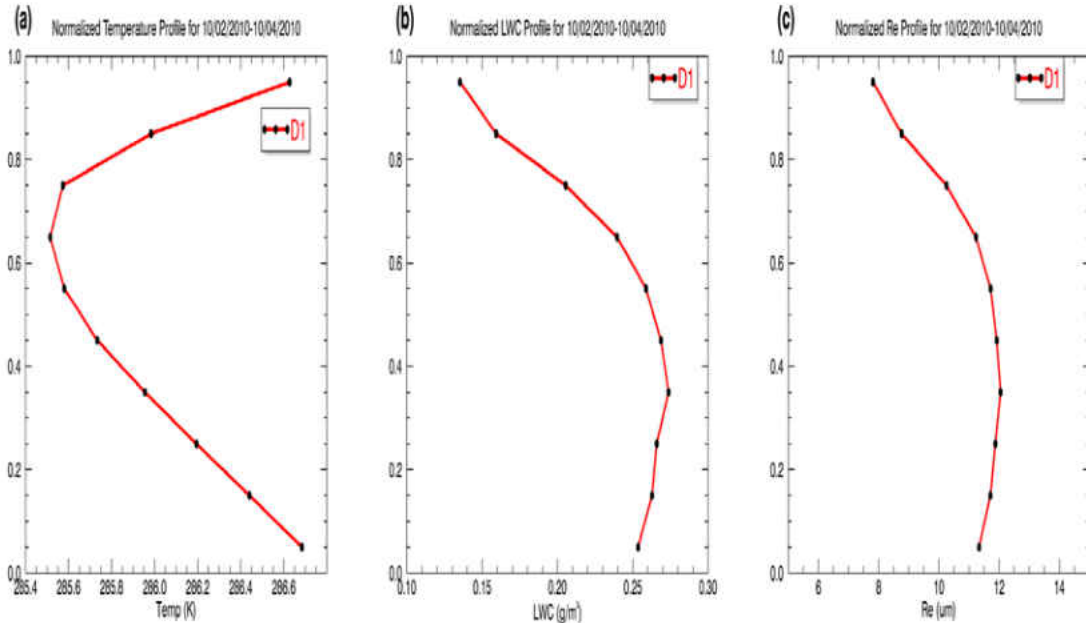


Figure 15. Normalized profiles of (a) temperature, (b) LWC, and (c) r_e , for the 2-4 October, 2010 case.

The stratocumulus cloud layer for the 21-22 October, 2009 case was initially coupled at the beginning of the period from 7:00-14:00 UTC, but decoupled for the rest of the period. In Figs. 16a and 16b, the cloud layer was relatively unbroken and thin during the coupled time period, but thickened and broke during the decoupled time period. The cloud structures and microphysical properties during the coupled and decoupled time periods are very similar to the corresponding properties in the above coupled, 2010 and decoupled, 2009 cases. That is, drizzling events are also more prevalent during the decoupled period compared to the coupled period. During the decoupled period of this case, LWP, r_e , and cloud thickness values were higher and fluctuated more frequently compared to the coupled period due to a large amount of drizzle events (Figs. 16a-d). During the coupled time period the N_d and N_{CCN} values were higher than those during the decoupled time period (Figs. 16e).

The normalized temperature profiles for this case (Fig. 17a) shows that the coupled period had an inversion layer ($\Delta T=2$ K) in the upper part of the cloud layer, while the decoupled period had no inversion layer within the cloud layer, which allowed the cloud layer to be thicker during the decoupled period. The normalized r_e and LWC profiles (Figs. 17b,c) for this case show that during the coupled period, both profiles slightly increased from the cloud base to the upper part of the cloud layer, then decreased sharply to the cloud top. For the decoupled time period, LWC and r_e monotonically decrease from the cloud base to the cloud top.

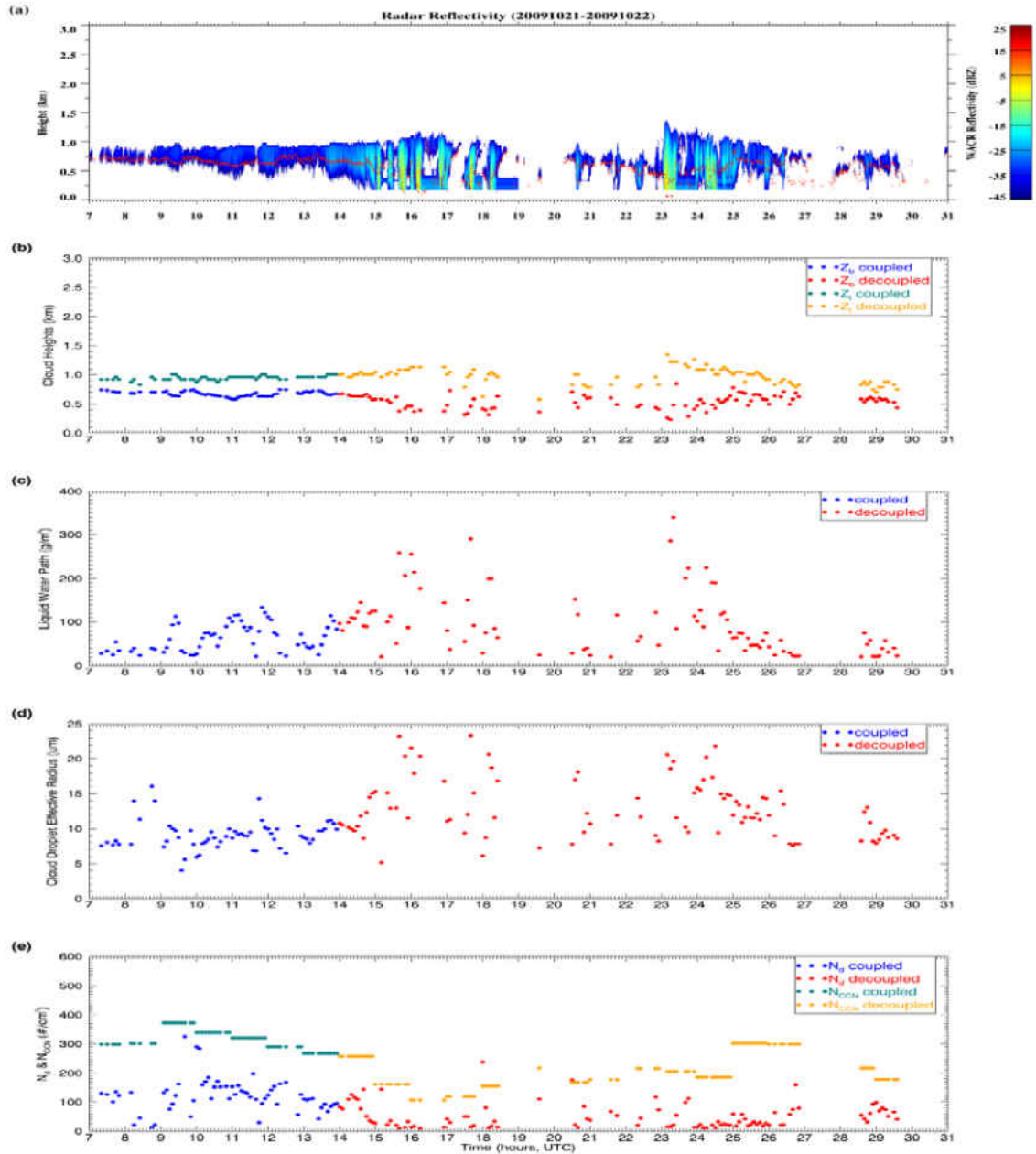


Figure 16. Time series of (a) radar reflectivity, (b) cloud-base (Z_b) and -top (Z_t) heights derived from ARM radar-lidar measurements, (c) cloud liquid water path (LWP) retrieved from microwave radiometer, (d) cloud-droplet effective radius (r_e), and (e) cloud droplet number concentration (N_d) and cloud condensation nuclei concentration (N_{CCN}) under conditions of coupled and decoupled during the 21-22 October, 2009 case.

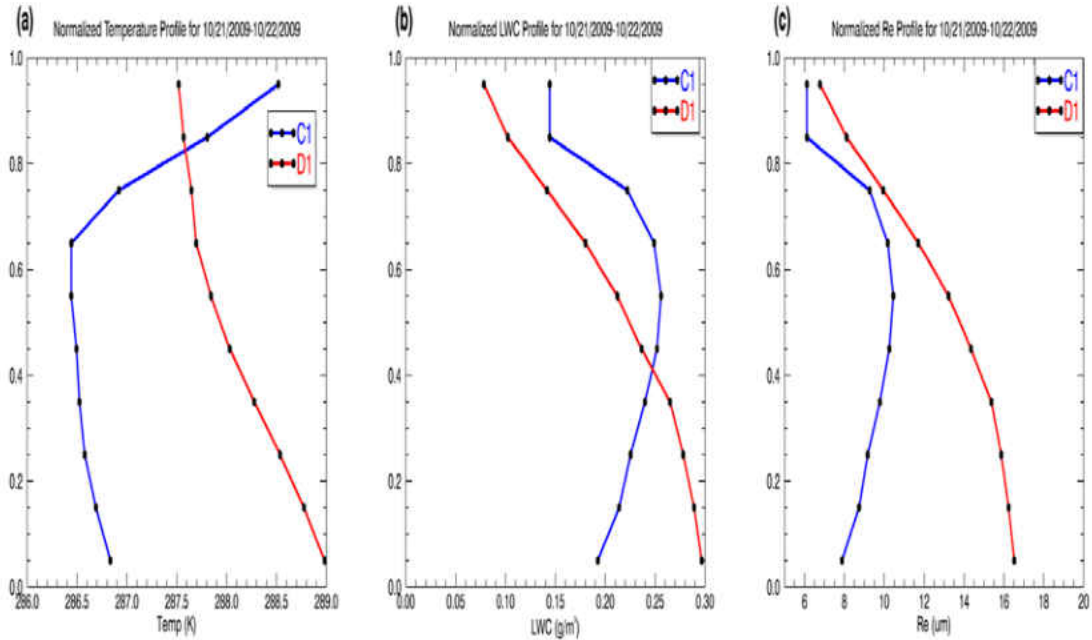


Figure 17. Normalized profiles of (a) temperature, (b) LWC, and (c) r_e for the 21-22 October, 2009 case. The red line is for the decoupled period and the blue line is for the coupled period.

Figs. 18-23 show three cases on 2-3 November, 2009, and 11-12 October, and 7-9 November, 2010, which are similar to the 21-22 October, 2009 case and include both coupled and decoupled time periods. Their cloud structures, microphysical properties, and normalized profiles are also similar to the cloud properties of the above coupled and decoupled cases, although there are slight differences from case to case. Therefore, it is unnecessary to discuss the details for each case.

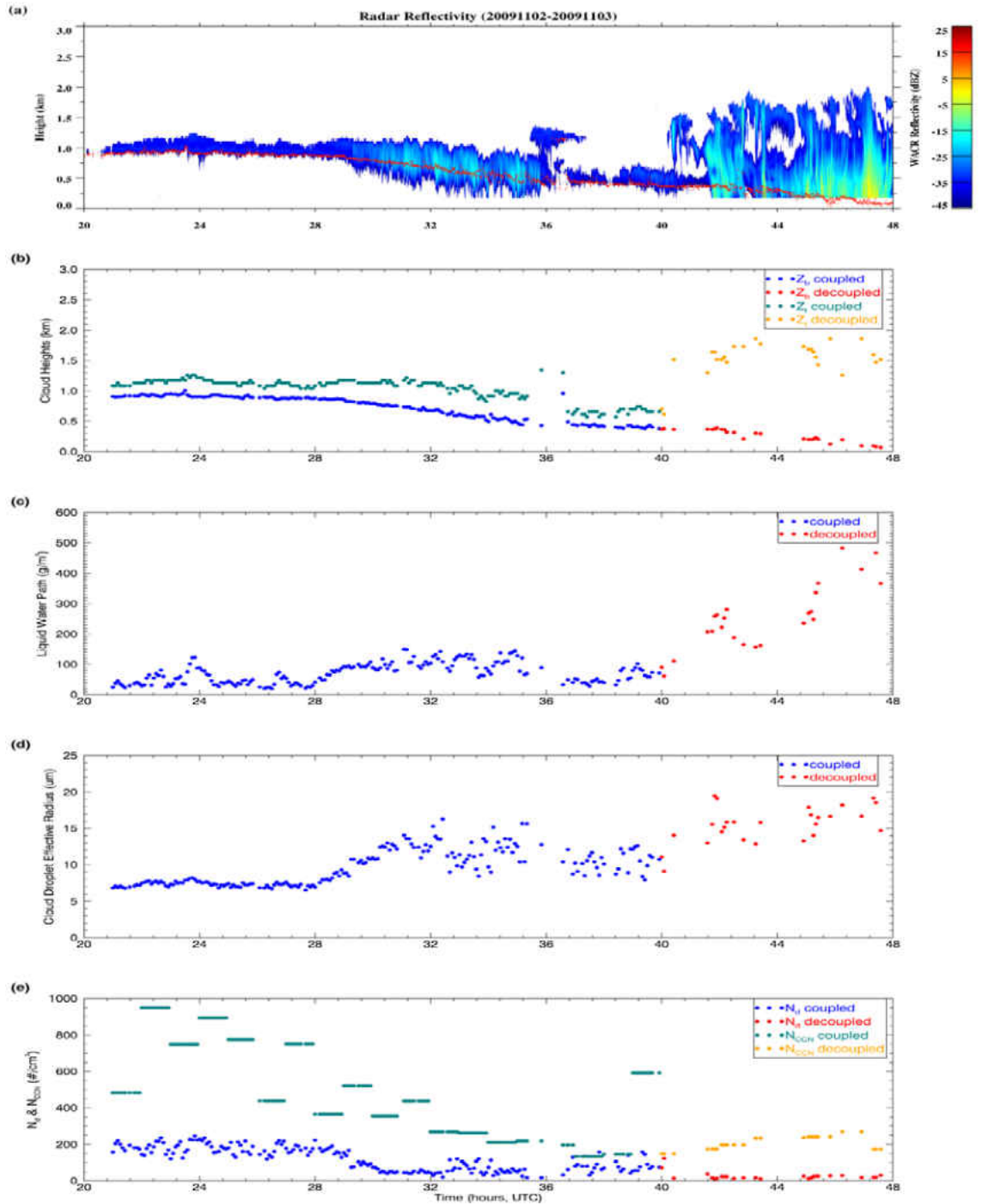


Figure 18. Time series of (a) radar reflectivity, (b) cloud-base (Z_b) and –top (Z_t) heights derived from ARM radar-lidar measurements, (c) cloud liquid water path (LWP) retrieved from microwave radiometer, (d) cloud-droplet effective radius (r_e), and (e) cloud droplet number concentration (N_d) and cloud condensation nuclei concentration (N_{CCN}) under conditions of coupled and decoupled during the 2-3 November, 2009 case.

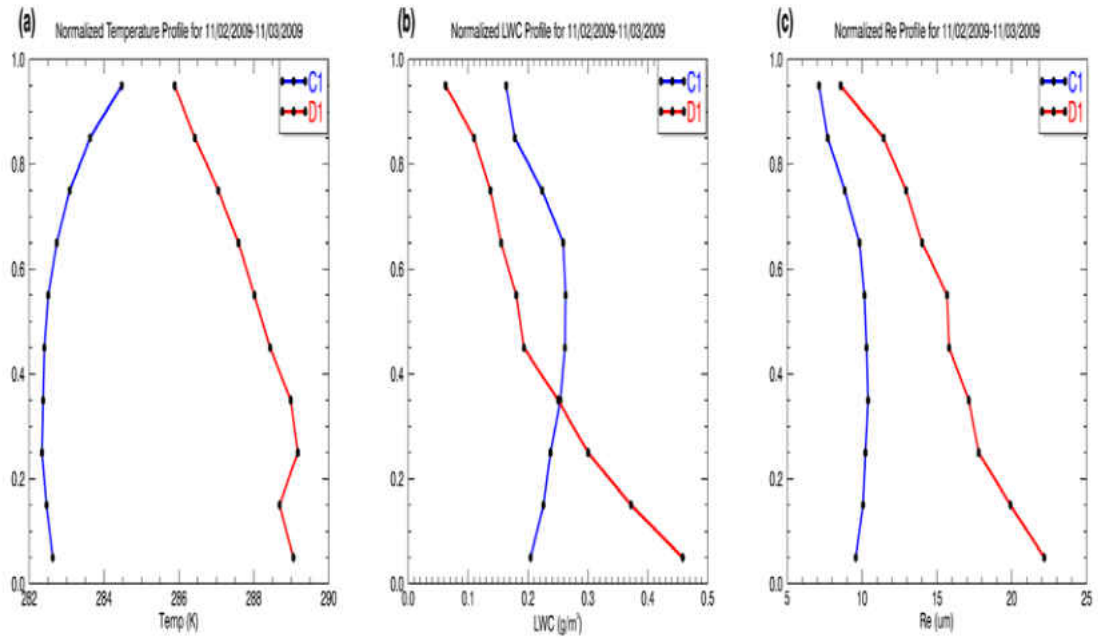


Figure 19. Normalized profiles of (a) temperature, (b) LWC, and (c) r_e , for the 2-3 November, 2009 case. The red line is for the decoupled period and the blue line is for the coupled period.

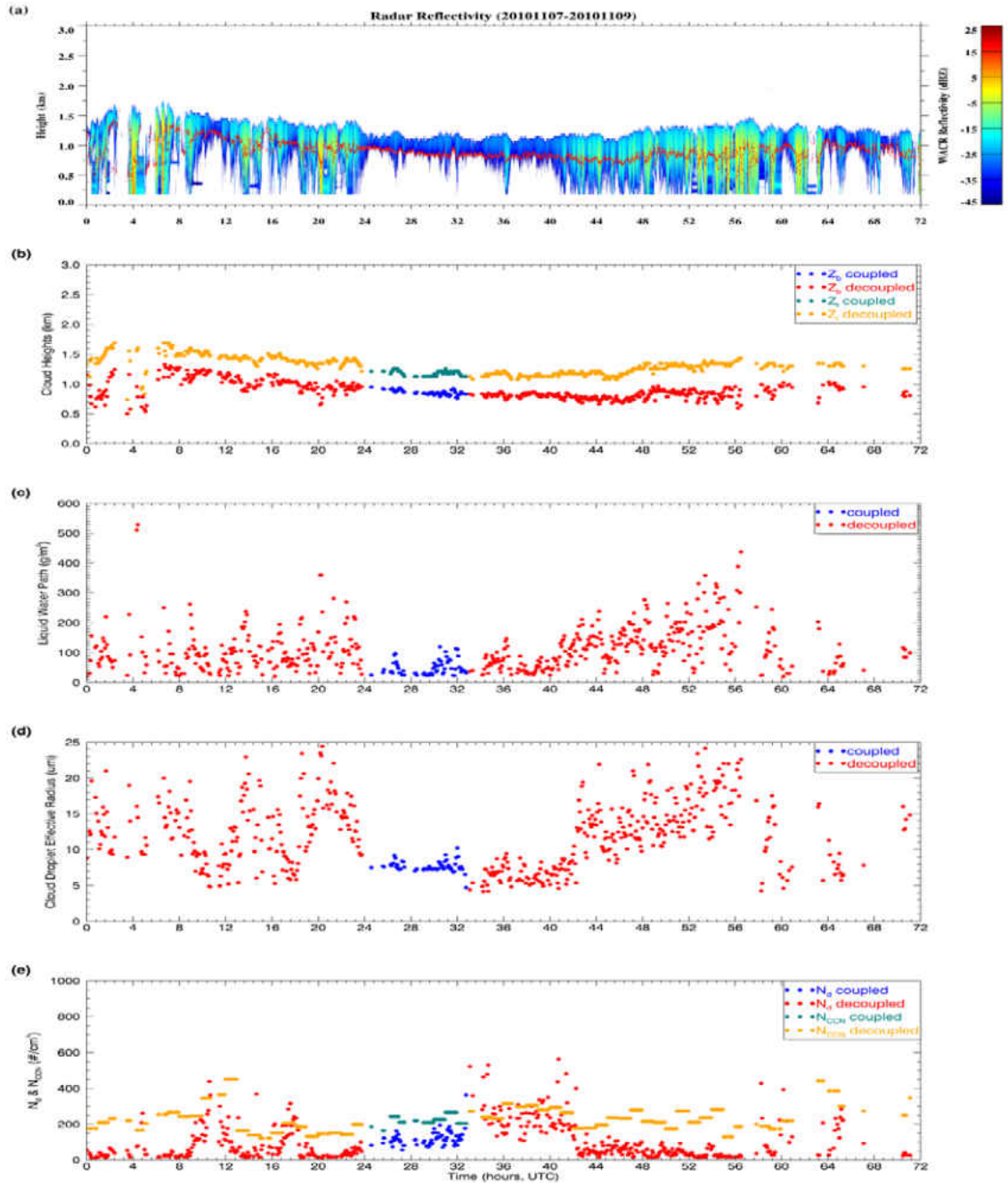


Figure 20. Time series of (a) radar reflectivity, (b) cloud-base (Z_b) and -top (Z_t) heights derived from ARM radar-lidar measurements, (c) cloud liquid water path (LWP) retrieved from microwave radiometer, (d) cloud-droplet effective radius (r_e), and (e) cloud droplet number concentration (N_d) and cloud condensation nuclei concentration (N_{CCN}) under conditions of coupled and decoupled during the 7-9 November, 2010 case.

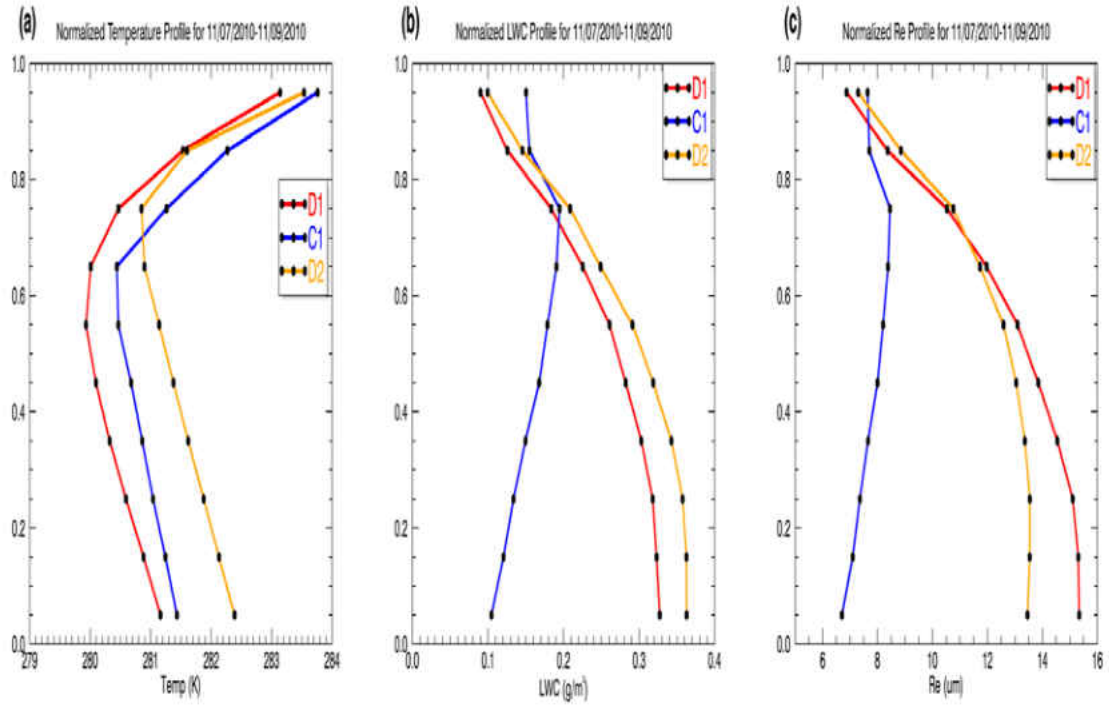


Figure 21. Normalized profiles of (a) temperature, (b) LWC, and (c) r_e for the 7-9 November, 2010 case. The red line is for the first decoupled period, the blue line is for the coupled period, and the orange line is for the second decoupled period.

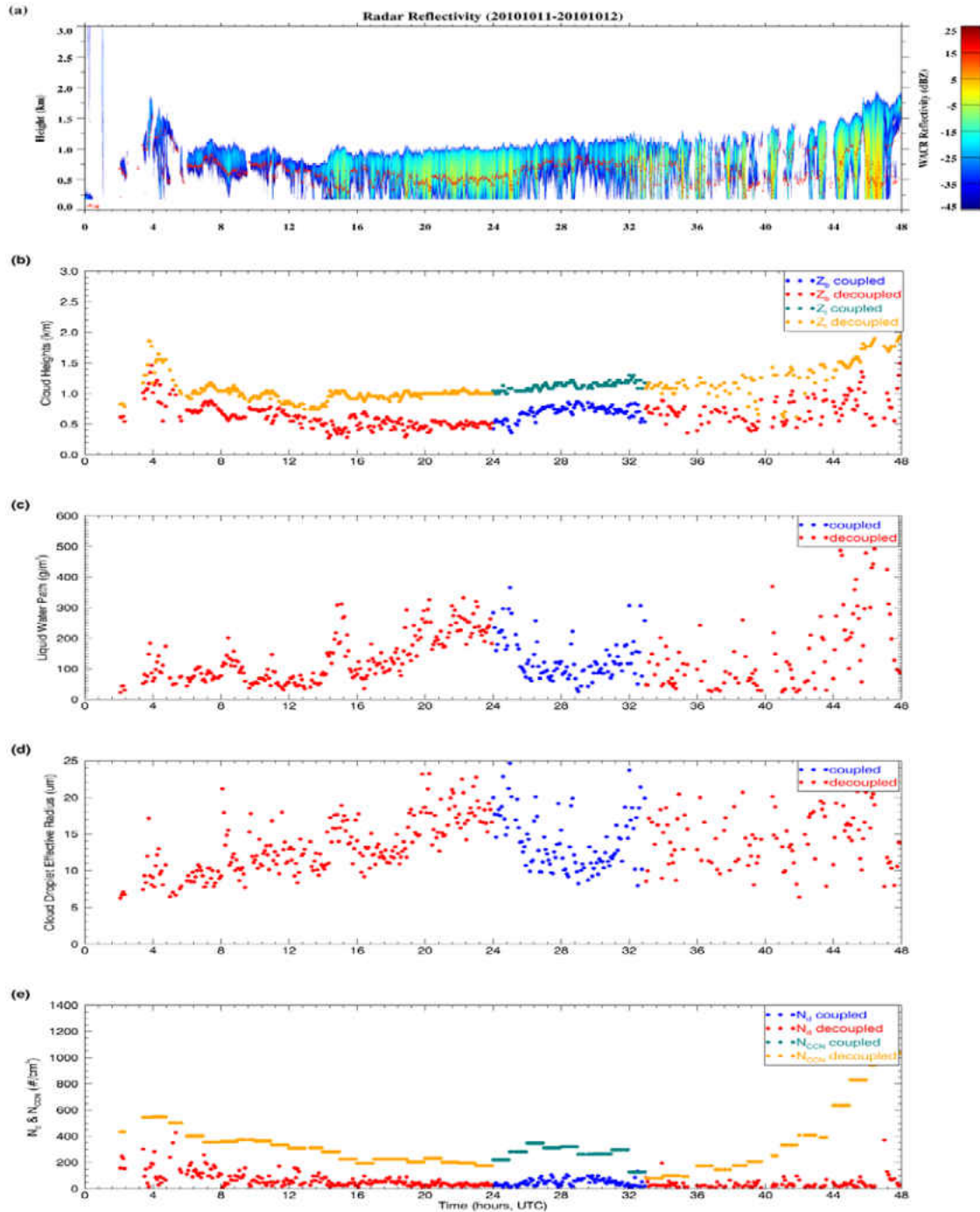


Figure 22. Time series of (a) radar reflectivity, (b) cloud-base (Z_b) and -top (Z_t) heights derived from ARM radar-lidar measurements, (c) cloud liquid water path (LWP) retrieved from microwave radiometer, (d) cloud-droplet effective radius (r_e), and (e) cloud droplet number concentration (N_d) and cloud condensation nuclei concentration (N_{CCN}) under conditions of coupled and decoupled during the period 11-12 October, 2010 case.

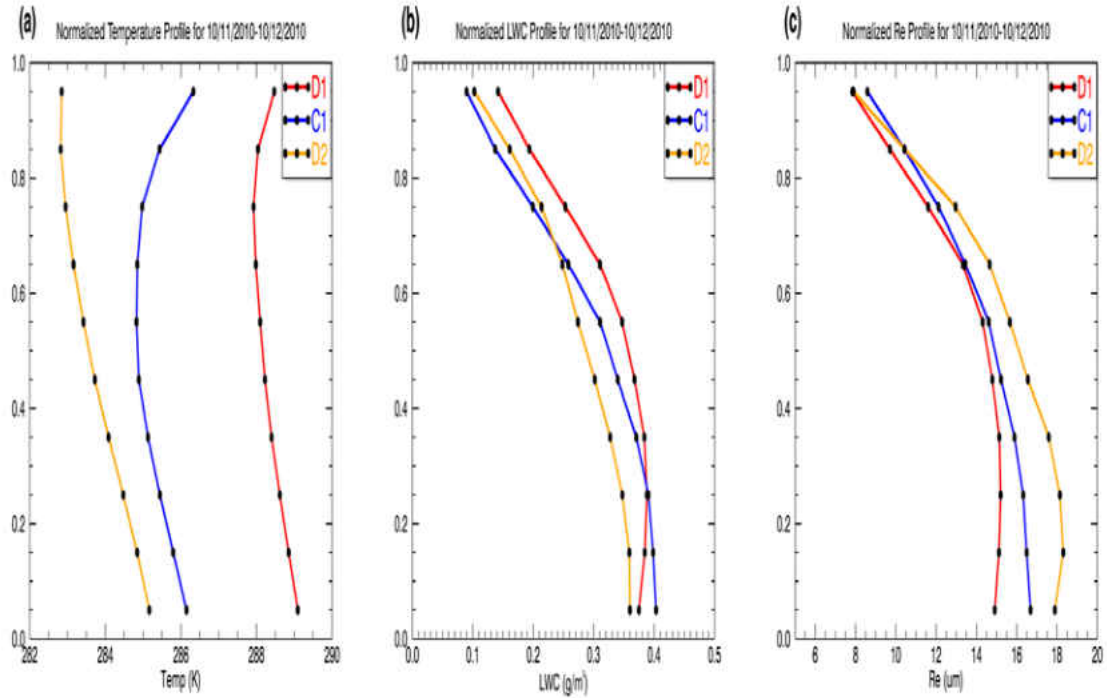


Figure 23. Normalized profiles of (a) temperature, (b) LWC, and (c) r_e for the 11-12 October, 2010 case. The red line is for the first decoupled period, the blue line is for the coupled period, and the orange line is for the second decoupled period.

In summary, the cloud layer was unbroken and thin for coupled periods with low cloud LWP and r_e values, along with high N_d and N_{CCN} values. Another finding is that both the cloud macro- and micro-physical properties are relatively stable with less fluctuations and drizzle for coupled periods. The decoupled periods have more heavy drizzle events, which results in larger fluctuations in the physical properties of the stratocumulus clouds, leading to higher LWP and r_e values, and lower N_d values. The cloud layer is also thicker during decoupled periods compared to coupled periods, because decoupled periods had either no inversion layer within the cloud, or were higher when compared to the coupled period inversion heights.

B. Statistics

Statistical results for the selected cases, including the mean, median, standard deviation, probability distribution (PDF), and cumulative distribution function (CDF), are provided in this section. The differences that are discussed in this section were found to be greater than the uncertainties of each instrument/method listed in Table 2. This section will be divided into three subsections, with different comparisons provided in each.

1. Coupled vs Decoupled

In this section, the statistical relationships between coupled and decoupled periods are analyzed. Figure 24 shows PDFs and CDFs of stratocumulus cloud macro-physical properties for both coupled (blue) and decoupled (red) periods. Tables 3-5 list the means, medians, and standard deviations of stratocumulus cloud macro-physical properties for both coupled and decoupled periods. The coupled distributions for averaged cloud temperatures, cloud base height, and cloud top height are all bimodal. The secondary peaks located in the 4 ° C to 6 ° C bin, 1.6 km - 1.8 km bin, and 1.2 km - 1.4 km bin for the coupled cloud temperature, cloud base height, and cloud top height distributions respectively, represent the 22-23 November 2009 case, which makes up 30% of all coupled samples. Despite being bimodal, the coupled distributions for cloud temperature and cloud base height are similar to the decoupled distributions, leading to the means and medians of the coupled and decoupled distributions being similar (Tables 4 and 5). Standard deviations for the decoupled cloud base heights and cloud temperatures were slightly higher compared to the coupled standard deviations (Table 6). Both cloud top height distributions had a maximum in the 1 - 1.2 km (37% coupled, 26% decoupled) bin. The decoupled cloud-top heights more values greater than 1.2 km (65%) compared to the

coupled distribution (50%), leading to a higher mean, median, and standard deviation than those from the coupled periods (Tables 3). The statistical significance of the mean difference between coupled and decoupled cloud top heights, however, cannot be determined by the Student's T-Test due to the coupled distribution being bimodal. The decoupled cloud thickness distribution is slightly more skewed towards higher values compared to the coupled distribution. This is consistent with the findings of the previous section, wherein decoupled stratocumulus clouds were thicker compared to coupled stratocumuli. The decoupled distribution has 45% of its cloud thickness values greater than 0.4 km, while the coupled distribution has only 15% above this threshold. The mean (314.4 m), median (304.5 m), and standard deviation (107.6 m) for the coupled cloud thickness values are lower compared to the decoupled mean (437.5 m), median (387.7 m), and standard deviation (232.5 m) (Tables 3). This agrees well with Jones et al. (2011) who found that decoupled stratocumuli were thicker than coupled stratocumuli. Using the Student T-Test it was determined that the mean difference between coupled and decoupled cloud thickness is statistically significant due to the p value being much less than 0.05, which is the confidence level. The calculated Cohen's d value (0.55) also shows that this mean difference has moderate practical significance.

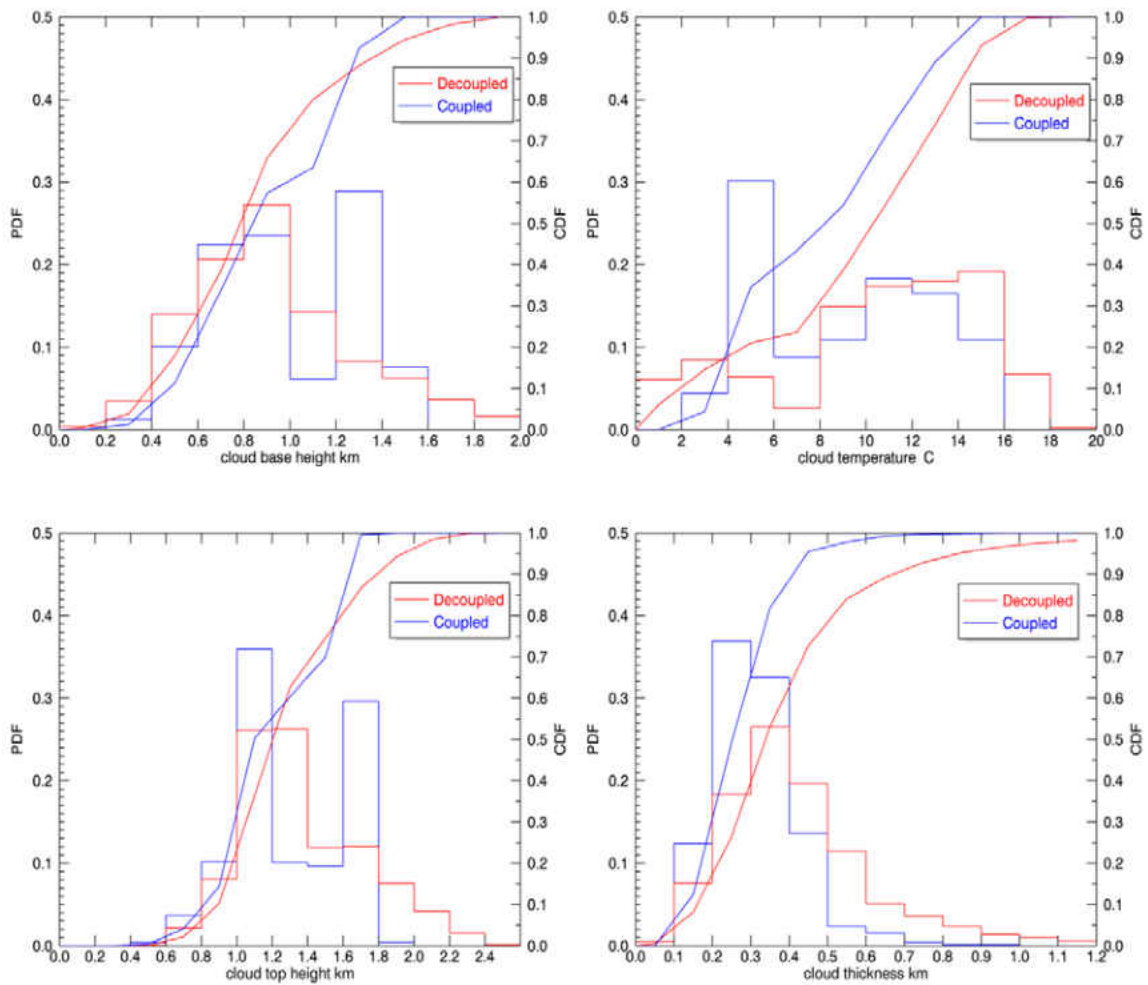


Figure 24. PDFs and CDFs of the coupled (blue) and decoupled (red) stratocumuli macrophysical properties for all cases.

Figure 25 shows the PDFs and CDFs of stratocumulus cloud micro-physical properties for both coupled (blue) and decoupled (red) periods. The decoupled distributions of N_{CCN} and N_d are skewed to lower values, while the coupled distribution is skewed to higher values. The decoupled N_{CCN} distribution has 40% of the values between $0-200 \frac{\#}{cm^3}$, while the coupled N_{CCN} distribution has only 15% of the values in this range. These findings are consistent with the previous section, wherein decoupled stratocumuli had lower N_{CCN} and N_d values compared to coupled stratocumuli. The

coupled N_{CCN} mean ($372.2 \frac{\#}{cm^3}$) and median ($329.7 \frac{\#}{cm^3}$) were higher than the decoupled mean ($268.3 \frac{\#}{cm^3}$) and median ($235.8 \frac{\#}{cm^3}$), which is consistent with the distributions shown in Fig. 25. The coupled N_{CCN} standard deviation was slightly lower compared to the decoupled N_{CCN} standard deviation due to the higher spread in decoupled values. The decoupled distribution of N_d concentrations have more small N_d concentrations ($< 100 \frac{\#}{cm^3}$) compared to the coupled N_d distribution for two reasons. The first reason is that the decoupled stratocumuli do not have N_{CCN} coming from the surface, which does not allow more cloud droplets to form. The second reason is that more decoupled stratocumuli were also drizzling 71% of the time compared to the coupled stratocumuli that were only drizzling 63% of the time. Drizzle is formed through the collision and coalescence of cloud droplets, which means the number of cloud droplets is greatly reduced when drizzle is present within a cloud. The mean difference between coupled and decoupled N_d values is statistically significant with the Student's T-Test derived p value being much less than 0.05. The Cohen's d value for the mean difference between coupled and decoupled N_d values is 0.7, indicating that the mean difference has moderate practical significance. The r_e and LWP distributions for the decoupled periods were skewed to high values, while the coupled distributions were skewed to low values. The decoupled LWP distribution has 20% of its values greater than $150 \frac{g}{m^2}$ while the coupled LWP distribution has only 3% of its values above this threshold. The coupled r_e distribution has most of its values between 6 and 14 μm (98%) while the decoupled r_e distribution has a broad range of values between 6- 22 μm with 55% of the values being greater than 12 μm . The decoupled r_e and LWP means, medians, and standard deviations

were higher than their coupled counterparts (Tables 3-5). Decoupled stratocumulus clouds had higher LWP and r_e values compared to the coupled stratocumuli because more drizzle events occurred when the cloud layer was decoupled. The mean differences between coupled and decoupled LWP and r_e values are both statistically significant with p values being much less than the confidence level (0.05). The Cohen's d values for the LWP and r_e values are 0.64 and 0.82 respectively, suggesting that the LWP mean difference has moderate practical significance and the r_e mean difference has large practical significance.

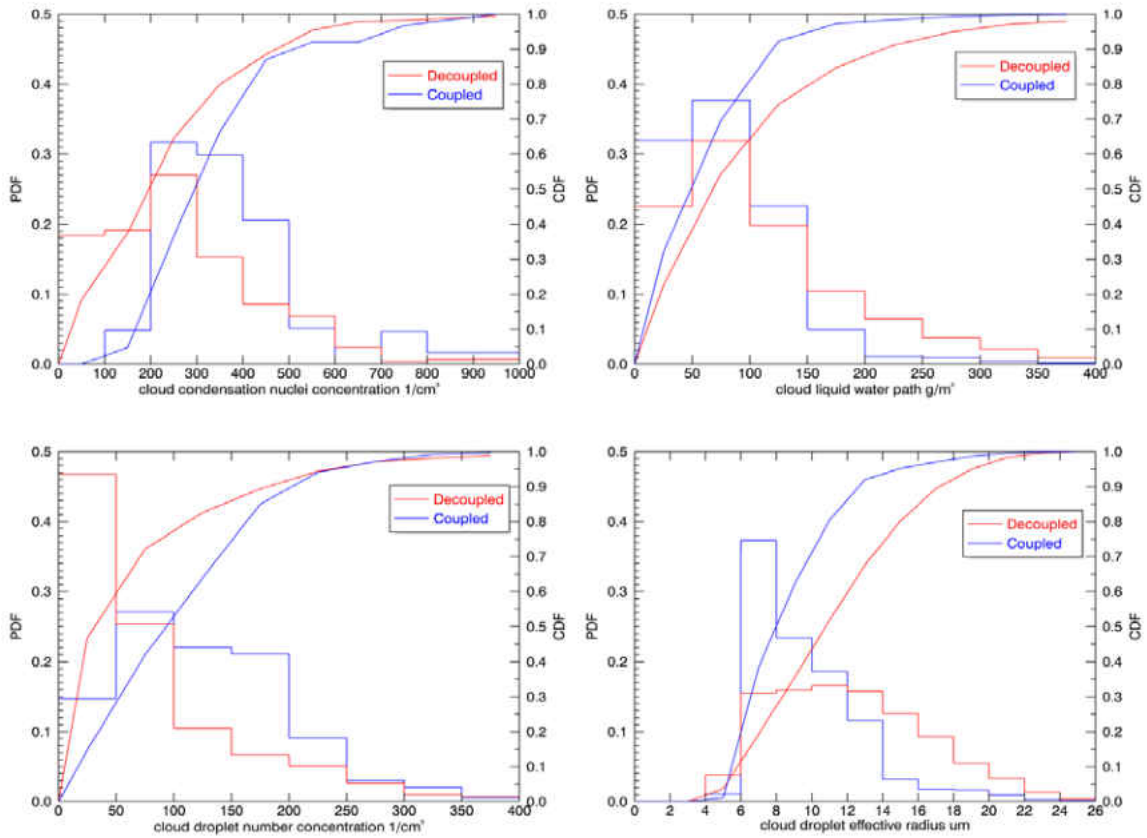


Figure 25. PDFs and CDFs of the day (blue) and night (red) stratocumuli micro-physical properties for all cases.

Table 4. Mean values of different cloud properties for coupled and decoupled stratocumuli.

Case Means Coupled (C) vs Decoupled (D)	C LWP	D LWP	C N_{CCN}	D N_{CCN}	C N_d	D N_d	C r_e	D r_e	C Zthick	D Zthick	C Zbase	D Zbase	C Ztop	D Ztop
10/21/09-10/22/09	64.6	90.1	315	223.3	132.1	38.6	9	13.7	273.7	409.9	670	572.3	943.5	982.2
11/02/09-11/03/09	66.7	277.68	464.1	205.5	107.3	28.3	9.7	15	287.4	1276.1	767.3	257.6	1054.7	1533.7
11/22/09-11/23/09	86.6	68.9	380.1	304.7	145.2	108.4	9.3	10.3	301.1	294.7	1325.8	1593.3	1626.9	1888.1
05/11/10-05/12/10	N/A	132.2	N/A	43.7	N/A	55.2	N/A	14.4	N/A	454.5	N/A	1344.6	N/A	1799.2
10/02/10-10/04/10	N/A	99.7	N/A	439.8	N/A	76.8	N/A	12.1	N/A	417.9	N/A	871.1	N/A	1289
10/11/10-10/12/10	131.5	139.5	270.7	340	27	45.2	16.5	14.7	427.4	454.2	696.6	649.3	1124	1103.4
11/07/10-11/09/10	50.5	115.8	226.6	230.6	101.9	95.2	8.1	12.1	327.5	414.6	856.7	899.3	1184.1	1314
Total Case Means	82.2	118.3	372.2	268.3	113.1	70.1	10.3	13.1	314.4	437.5	978.5	926.8	1293	1364.3

Table 5. Median values of different cloud properties for coupled and decoupled stratocumuli.

Case Median Coupled vs Decoupled	C LWP	D LWP	C N_{CCN}	D N_{CCN}	C N_d	D N_d	C r_e	D r_e	C Zthick	D Zthick	C Zb	D Zb	C Zt	D Zt
10/21/09-10/22/09	63.4	66.9	321.2	206.2	112.7	30.2	9.5	13	272.4	374.2	670.6	579.1	958.4	1001.3
11/02/09-11/03/09	59.7	258.6	437.1	197.5	116.6	22.1	8.5	14.7	259.7	1393.5	858	297.2	1129.9	1601.3
11/22/09-11/23/09	75.9	56	379.2	297.3	139	77.5	8.7	10.4	290.5	272	1328.9	1589.1	1644.1	1901.3
05/11/10-05/12/10	N/A	105.7	N/A	33.8	N/A	35.2	N/A	14.5	N/A	399.7	N/A	1290.8	N/A	1729.9
10/02/10-10/04/10	N/A	73.4	N/A	411	N/A	60.3	N/A	10.6	N/A	337.1	N/A	887.6	N/A	1258.4
10/11/10-10/12/10	114.2	105.9	283.2	309.8	24.6	35.2	16	13.6	417	438.3	712.1	607.9	1129.9	1001.3
11/07/10-11/09/10	43.6	101.4	226.6	220.5	99	49.5	7.9	12.8	311.8	400.7	851.5	867.2	1172.7	1301.3
Total Case Medians	72.9	91.6	329.7	235.8	108.4	42.7	9.1	12.8	304.5	387.7	901.9	875	1172.7	1301.3

Table 6. Standard deviation values of different cloud properties for coupled and decoupled stratocumuli.

Case Stdev Coupled vs Decoupled	C LWP	D LWP	C N_{CCN}	D N_{CCN}	C N_d	D N_d	C r_e	D r_e	C Zthick	D Zthick	C Zb	D Zb	C Zt	D Zt
10/21/09-10/22/09	31.8	76.2	34.3	69.5	112.1	34.7	1.6	4.	64.8	198.5	41.7	152.8	35.8	137
11/02/09-11/03/09	34.1	135.6	250.9	37.6	50	23.3	2.3	2.2	107.1	352.7	209.8	105.7	184.9	300.9
11/22/09-11/23/09	48.6	44.8	73.5	43.6	70.4	89.1	2.3	3.2	95.9	106.7	101.5	85.4	69.3	77.8
05/11/10-05/12/10	N/A	100.8	N/A	24.1	N/A	100	N/A	4.1	N/A	246.3	N/A	293.9	N/A	278.7
10/02/10-10/04/10	N/A	86.7	N/A	150.3	N/A	71.5	N/A	4.2	N/A	248	N/A	234.6	N/A	248.6
10/11/10-10/12/10	69	100	62.2	206.8	11.6	34.2	3.4	4.1	111.5	216.8	109.8	209.6	64.9	261.1
11/07/10-11/09/10	25.7	74.9	25	70.3	26.6	98.1	0.6	4.1	52.7	111.4	41.7	151.6	43.1	151.6
Total Case Standard Deviations	51.1	92.1	165.6	183.1	72.9	82.5	3.4	4.3	107.6	232.5	315	353.2	298.6	347

2. Drizzle vs Non-Drizzle

In this section, the statistical relationships between drizzling and non-drizzling clouds during coupled and decoupled periods are analyzed. Figure 26 shows the PDFs and CDFs of stratocumulus cloud macrophysical properties for both non-drizzling (left) and drizzling (right) during coupled (blue) and decoupled (red) periods. Table 7 shows the means and standard deviations of stratocumulus cloud macrophysical properties. The drizzling/non-drizzling distributions of cloud base height and cloud temperature are nearly identical to each other, which is why the means and standard deviations for these properties are nearly identical as well. The coupled and decoupled drizzling distributions of cloud top heights are skewed towards high values, with 50% and 65% of the values being greater than 1.2 km respectively. The coupled and decoupled non-drizzling cloud top height distributions are skewed to low values with only 40% and 50% of the values being above 1.2 km. The coupled and decoupled non-drizzling distributions of cloud thickness are slightly skewed toward lower values, with 95% and 75% of their values between 0.1-0.4 km respectively, while the coupled and decoupled drizzling distributions

of cloud thickness have 95% and 70% of their values between 0.2-0.5 km respectively. The coupled/decoupled drizzling and non-drizzling cloud thickness distributions have a mean difference of 94.2 *m* and 116.2 *m* respectively. These cloud thickness mean differences are statistically significant, with *p* values much less than 0.05. These mean differences are also practically significant, with Cohen's *d* values of 1 and 0.53 respectively. The coupled non-drizzling/drizzling mean difference is more practically significant compared to its' decoupled counterpart, because the coupled non-drizzling/drizzling distributions have lower standard deviations. This is consistent with the previous section, wherein the cloud layer thickened when drizzle was present.

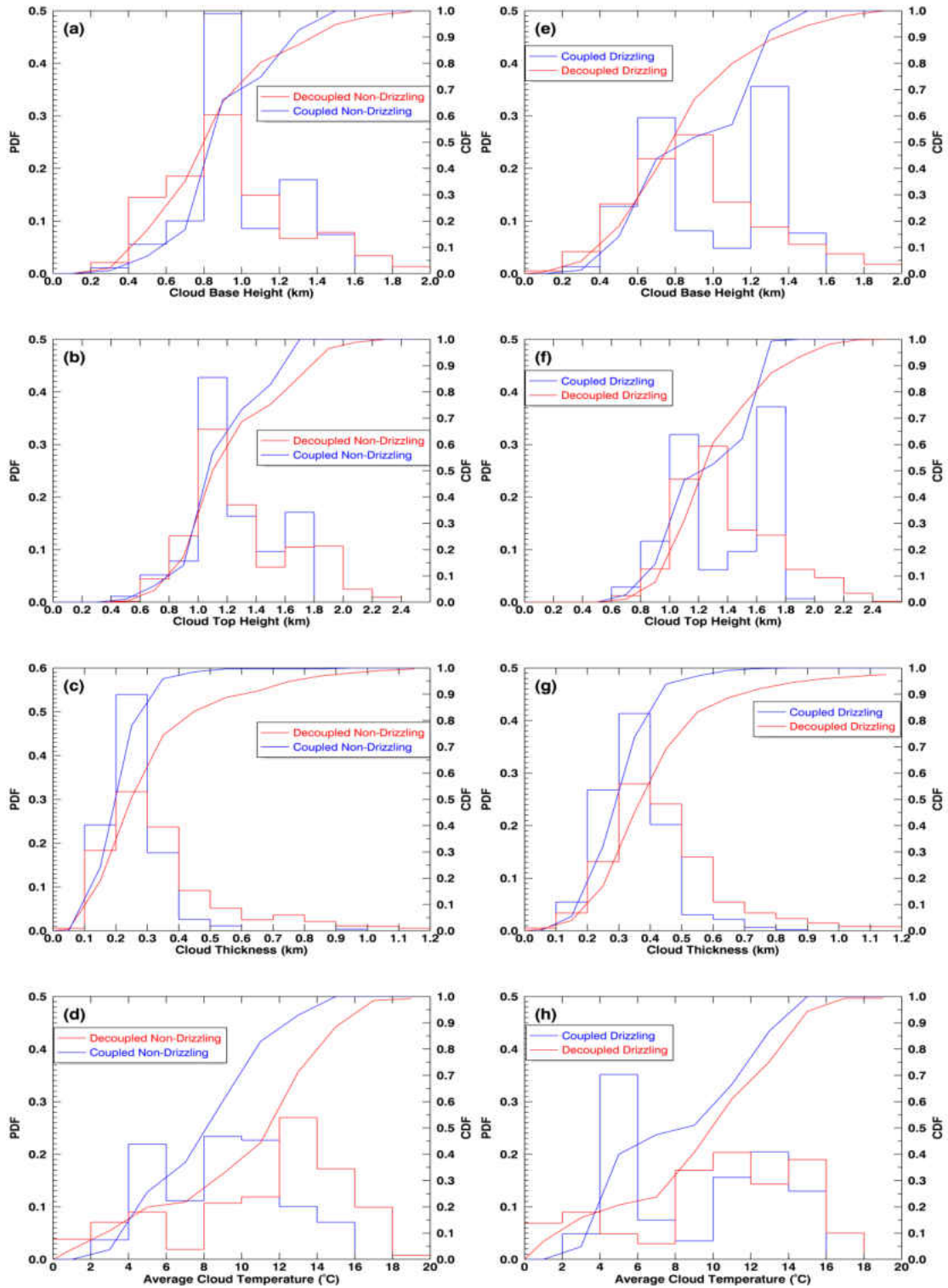


Figure 26. PDFs and CDFs of the coupled(blue)/decoupled(red) non-drizzling (left) and drizzling (right) stratocumuli macro-physical properties for all cases.

In Fig. 27, the N_{CCN} distributions for drizzling stratocumulus clouds are skewed toward low values while the non-drizzling distributions are skewed toward high values for both coupled and decoupled stratocumulus clouds. The decoupled drizzling N_{CCN} distribution has 70% of its values between 0-300 $\frac{\#}{cm^3}$ while the decoupled non-drizzling distribution only has 45% in this range. The coupled N_{CCN} distributions of drizzling and non-drizzling stratocumulus clouds show the same trends as the decoupled distributions, with higher N_{CCN} values being present in the non-drizzling distribution compared to the drizzling distribution. The trends seen in the N_{CCN} distributions are also seen in the N_d distributions. For both the coupled and decoupled drizzling N_d distributions, samplers are skewed toward lower values (0-100 $\frac{\#}{cm^3}$), while the non-drizzling N_d distributions are spread more evenly, resulting in a greater amount of high values. This is likely a result of drizzle droplets collecting smaller cloud droplets, thus decreasing the overall cloud droplet concentration. The means for both coupled and decoupled non-drizzling N_d values were higher compared to their coupled and decoupled drizzling N_d counterparts. These mean differences are statistically significant, with both differences having p values much less than 0.05. The coupled drizzling/non-drizzling N_d mean difference has a moderate practical significance with a Cohen's d value of 0.76, while the decoupled drizzling/non-drizzling N_d mean difference has small practical significance with a Cohen's d values of only 0.44. The difference between the decoupled drizzling/non-drizzling mean N_d values is less statistically significant compared to the coupled drizzling/non-drizzling mean difference due to higher standard deviations. The coupled and decoupled drizzling distributions for LWP and r_e are skewed to high values, while the non-drizzling distributions are skewed to lower values. The coupled and decoupled

LWP distributions for non-drizzling clouds have 85% and 95% of their values between 0-100 $\frac{g}{m^2}$ respectively, while the drizzling distributions only have 55% and 45% its values in this range respectively. This is consistent with the findings of other studies (Wood 2004, Remillard et al. 2012). The r_e distributions for coupled and decoupled non-drizzling stratocumuli are skewed to lower values, while the drizzling r_e distributions are skewed to higher values. Coupled drizzling stratocumulus clouds tend to have lower r_e values compared to decoupled drizzling clouds, which suggests that heavier drizzle was present when the cloud layer was decoupled from the surface compared to when it was coupled. The coupled/decoupled drizzling means for LWP and r_e are higher than their non-drizzling counterparts (Tables 7). These mean differences are all statistically significant, with p values much less than 0.05. The coupled drizzling and non-drizzling mean differences for LWP and r_e have large practical significance, with Cohen's d values of 1 and 1.2 respectively. The decoupled drizzling and non-drizzling mean differences for LWP and r_e also have large practical significance, with Cohen's d values of 0.98 and 1.1 respectively. The differences between non-drizzling and drizzling means for LWP, and r_e were greater compared to the coupling and decoupling mean differences, which suggests that drizzle has a greater effect on cloud micro-physical properties (except N_d) than whether a cloud is coupled or decoupled from the surface.

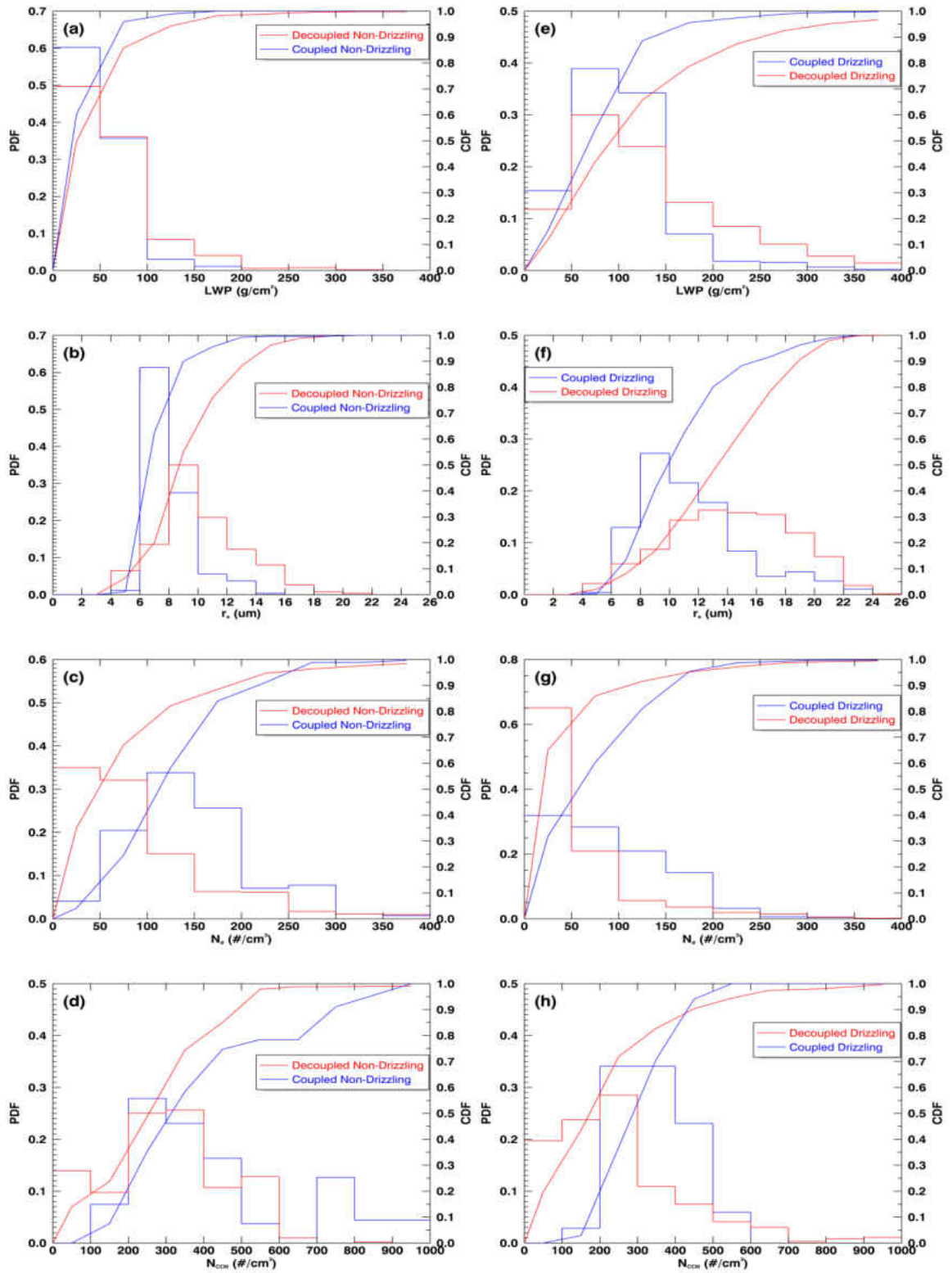


Figure 27. PDFs and CDFs of the coupled(blue)/decoupled(red) non-drizzling (left) and drizzling (right) stratocumuli micro-physical properties for all cases.

Table 7. Mean and standard deviation values of different cloud properties for drizzling and non-drizzling stratocumuli.

	Drizzling			Non-Drizzling	
	Coupled	Decoupled		Coupled	Decoupled
Mean z _b (m)	982.7	919.2		973.2	944.8
Std	339.3	355.7		269.8	346.2
Mean z _t (m)	1331.8	1388		1228.2	1297.4
Std	310	335.3		267.5	362.2
Mean Δz (m)	349.1	468.8		254.9	352.6
Std	105.3	234.2		81.2	206.8
Mean T _{cldy} (K)	283.3	282.2		282	284.1
Std	4.6	4		3.1	4.6
Mean LWP $(\frac{g}{m^2})$	100.6	141.9		50.9	64.6
Std	53.5	100.2		25.6	49.4
Mean r _e (μm)	11.6	14.3		8.2	10.2
Std	3.6	4.2		1.6	2.94
Mean N _d $(\frac{\#}{cm^3})$	93.8	59.7		145.7	95.9
Std	69.9	78.2		66.1	87
Mean NCCN $(\frac{\#}{cm^3})$	341	251.5		426.9	305
Std	92.3	184.2		233.8	171.8

3. Day vs Night

The night and day distributions of cloud temperature, cloud base and cloud top heights are similar to each other, because both day and night both have nearly equal amounts of drizzle (68% and 70%). This leads to the day and night means for these properties also being very similar (Tables 8). Overall, there are no significant differences of MBL cloud macro-physical properties between day and night periods except for cloud thickness, which is slightly greater during the night than during the day for both coupled and decoupled clouds (Fig. 28). The mean difference between the decoupled daytime and nighttime cloud thickness distributions is statistically significant, with a p-value much less than 0.01. This mean difference also has moderate practical significance with a Cohen's *d* value of 0.55.

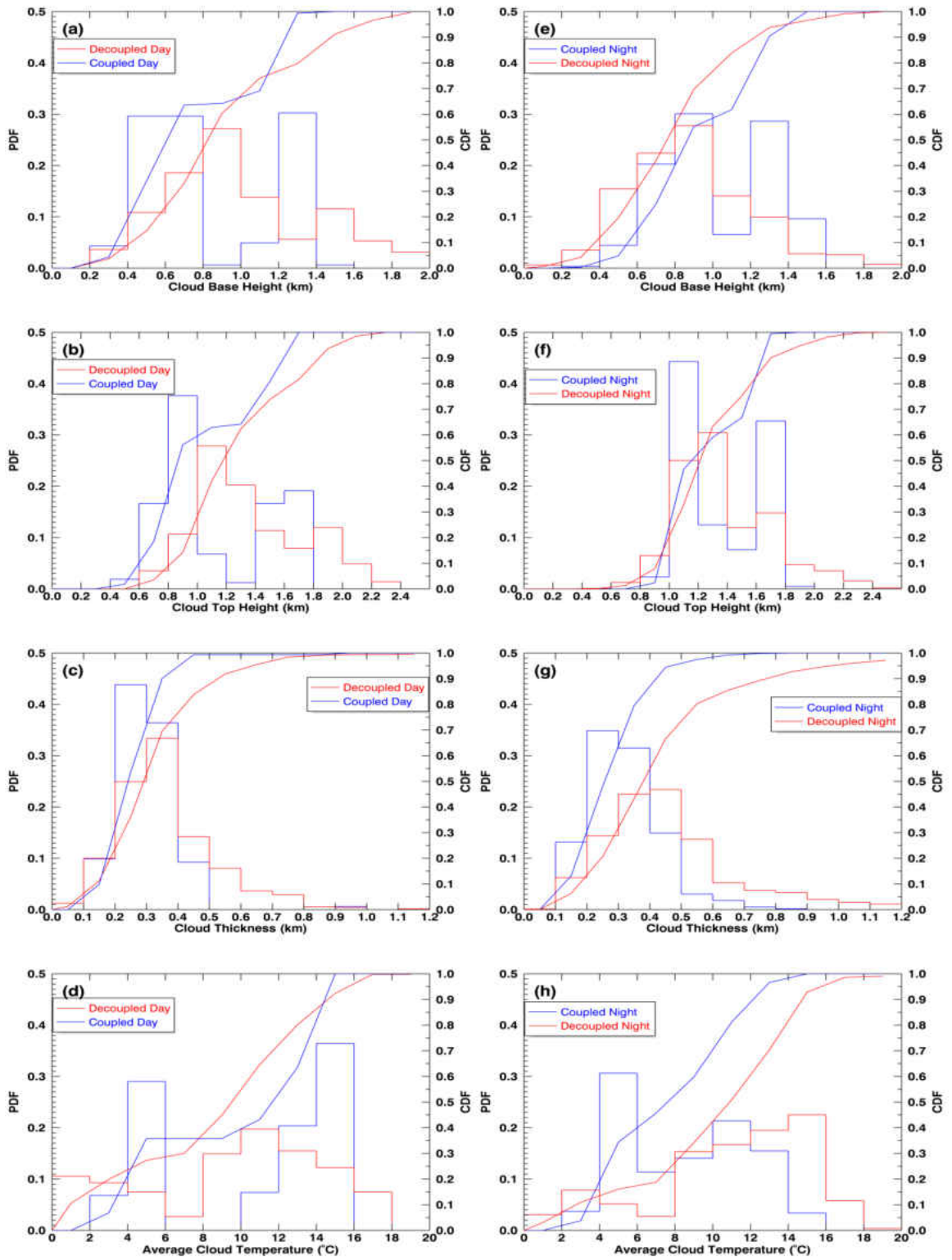


Figure 28. PDFs and CDFs of the coupled (blue)/decoupled (red) day (left) and night (right) stratocumuli macro-physical properties for all cases.

The microphysical properties of daytime coupled stratocumulus clouds did not vary significantly from their nighttime counterparts. The microphysical properties of daytime and nighttime decoupled stratocumulus clouds did, however, vary significantly. The decoupled N_{CCN} distributions for nighttime and daytime are relatively comparable, but the nighttime distribution has more N_{CCN} values greater than $500 \frac{\#}{cm^3}$ (15%) compared to the daytime N_{CCN} distribution (<5%). These values are mostly from the night of 12 October 2010, when there was a sharp increase in N_{CCN} concentrations (up to $1000 \frac{\#}{cm^3}$). The decoupled nighttime LWP distribution tends to have higher values compared to the daytime decoupled distribution. The night decoupled distribution of LWP has 35% of its values greater than $150 \frac{g}{m^2}$ while the day decoupled distribution has 5% above this threshold. The decoupled nighttime mean LWP is higher compared to the decoupled daytime mean. The difference between the decoupled day and night LWP means distribution was statistically significant with a p-value much less than 0.01. This mean difference also has moderate practical significance, with a Cohen's d value of 0.64. The decoupled N_d distribution for daytime has higher values compared to the decoupled nighttime distribution. The decoupled nighttime N_d distribution has 70% of its values between $0-100 \frac{\#}{cm^3}$, while the decoupled daytime N_d distribution only has 35% of its values within this threshold. The daytime and nighttime decoupled r_e distributions showed similar trends as the N_d distributions, but with the nighttime having higher r_e values compared to the daytime. This suggests there was heavier precipitation present for nighttime decoupled stratocumuli compared to daytime decoupled stratocumuli. The mean differences for decoupled daytime and nighttime distributions of N_d and r_e are both

statistically significant with p -values much less than 0.01, and have moderate/large practical significance, with Cohen's d -values of 0.7 and 0.82 respectively. With the exception of N_d and r_e , all of the standard deviations for nighttime decoupled cloud microphysical properties except for N_d are higher than those for daytime decoupled cloud properties.

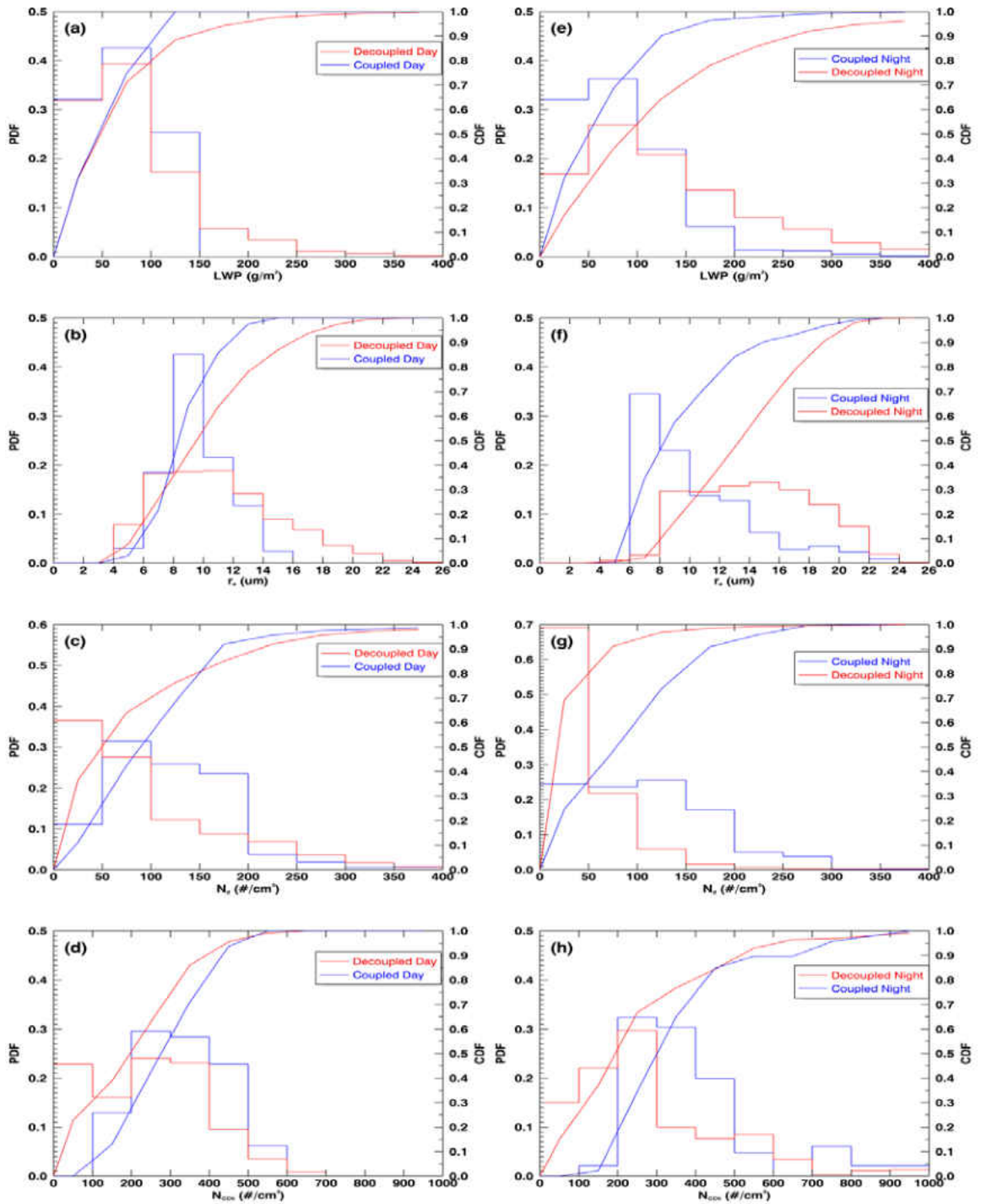


Figure 29. PDFs and CDFs of the coupled (blue)/decoupled (red) day (left) and night (right) stratocumuli micro-physical properties for all cases.

Table 8. Mean and standard deviation values of different cloud properties for daytime and nighttime stratocumuli.

	Day			Night	
	Coupled	Decoupled		Coupled	Decoupled
Mean z _b (m)	826.3	994.8		1023.3	882.8
Std	367.5	387.9		283.7	321.5
Mean z _t (m)	1126.2	1358.5		1341.4	1364.1
Std	369.1	372		256.3	327.6
Mean Δz (m)	299.9	363.7		318.2	481.3
Std	92.6	163.2		110.8	257.6
Mean T _{cdy} (K)	283.6	282.7		281.7	284
Std	4.6	4.9		3.27	4.3
Mean LWP ($\frac{g}{m^2}$)	73.5	85.5		84.6	141.5
Std	32.7	61.2		55.1	106.1
Mean r _e (μm)	9.5	11.1		10.5	14.4
Std	2.1	4		3.7	4
Mean N _d ($\frac{\#}{cm^3}$)	125	105.5		109.6	47.5
Std	89.8	110.1		67	45.5
Mean NCCN ($\frac{\#}{cm^3}$)	325.5	241.9		386.6	282.9
Std	118.3	149.2		174.3	199.1

C. Stratocumulus Cloud Layer Lifetime

Surface-based instruments are useful for examining the micro- and macrophysical properties of clouds that are directly overhead of the instruments. They cannot, however, provide information regarding the entire cloud layer at the same time. This is why satellite observations are important for investigating large weather systems — they can be

used to collect measurements over large areas at a single time. It is for this reason that satellite imagery is used to investigate whether stratocumulus layers are opened or closed celled for the selected cases. For this subsection only the 11-12 October, 2010 case is analyzed because it is the only case for which continuous satellite data are available. The weather system that was present during this case lasted four days (11-14 October, 2010), so the satellite images for all of these days are investigated.

1. Satellite Images

Total cloud fraction satellite data from Meteosat-9 are used to analyze the cloud layer from 11-14 October, 2010. These data are hourly and are distributed on grid box of $0.5^{\circ} \times 0.5^{\circ}$. If the cloud fraction is less than 0.9, then the stratocumulus layer is considered opened cell, otherwise the stratocumulus layer is considered closed cell.

On 11 October, 2010, the stratocumulus layer was decoupled from the surface for the whole day. The stratocumulus layer over the Azores was relatively unbroken during the early morning hours, but the layer began to break apart in the early afternoon, especially south of the Azores (Fig. 29). The cloud layer then began to reform during the night hours. There was one small patch of low cloud fraction just south of the Azores, which can be attributed to orographic lifting caused by Mount Pico.

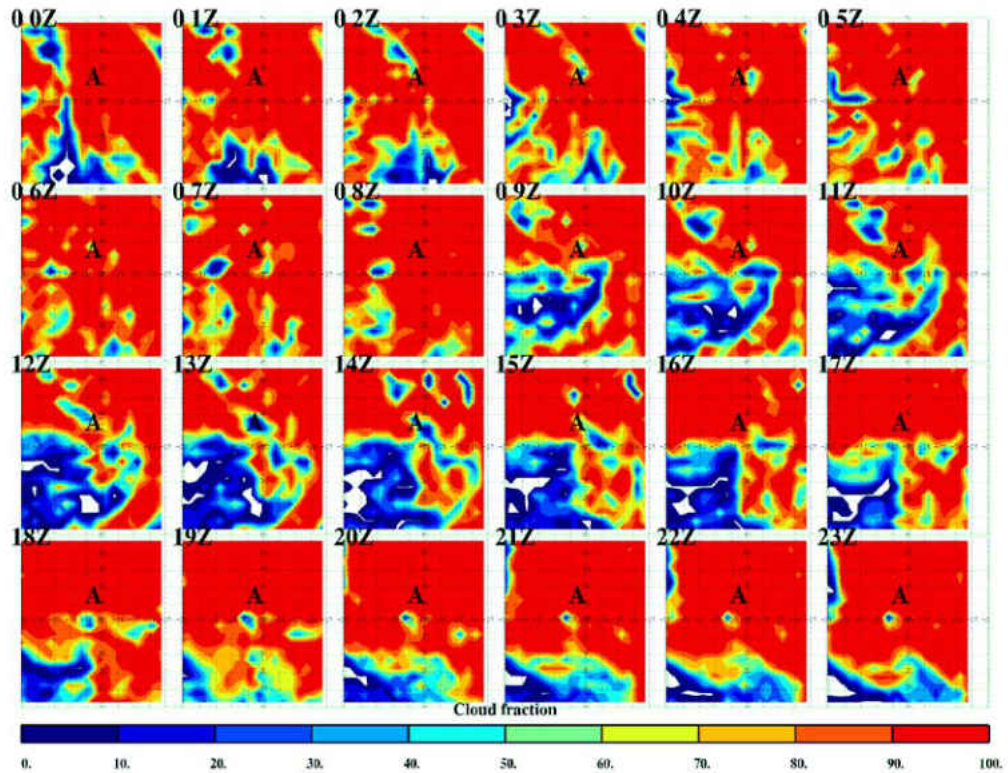


Figure 30. Hourly total cloud fraction images from Meteosat-9 over the Azores (A) on 11 October, 2010.

On October 12, 2010, the stratocumulus layer over the Azores was coupled to the surface from 0:00-9:00 UTC. During this period, the cloud layer remained unbroken except for a few locations (Fig. 30). During the afternoon, the cloud layer once again began to break apart to the west and north of the Azores. During the evening hours, the stratocumulus layer reformed, but open areas were present to the west of the Azores.

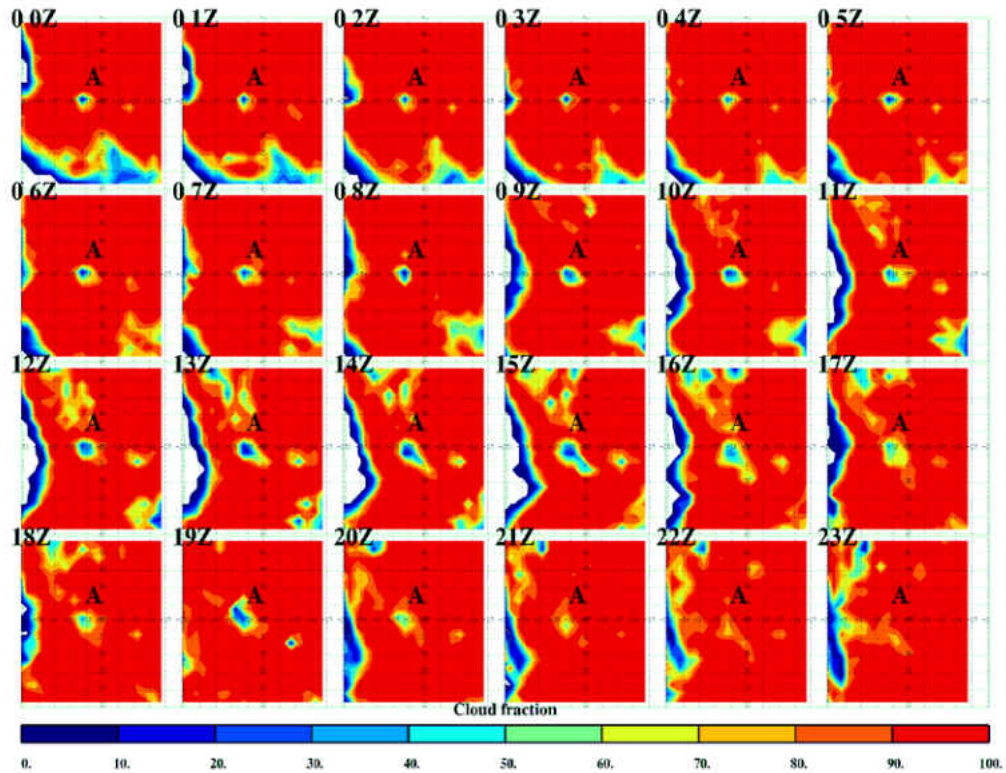


Figure 31. Hourly total cloud fraction images from Meteosat-9 over the Azores (A) on 12 October, 2010.

On 13 October, 2010, the stratocumulus layer over the Azores was decoupled for the whole day. During the early morning, the cloud layer was relatively unbroken, except for an area west of the Azores (Fig 31). The cloud layer then broke up significantly during the daylight hours. Once the sun set, the stratocumulus recovered slightly, but was still broken over the whole region.

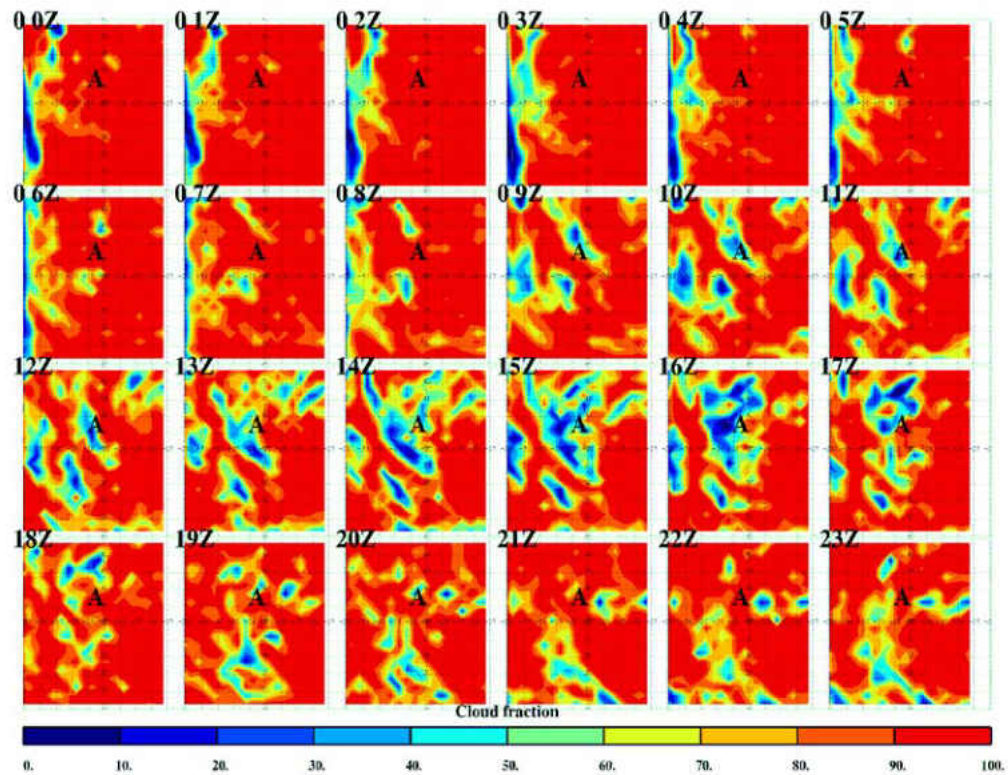


Figure 32. Hourly total cloud fraction images from Meteosat-9 over the Azores (A) on 13 October, 2010.

Finally on 14 October, 2010, the stratocumulus layer was broken for the whole day, especially during the afternoon. The cloud layer over the Azores was decoupled from the surface for the whole day.

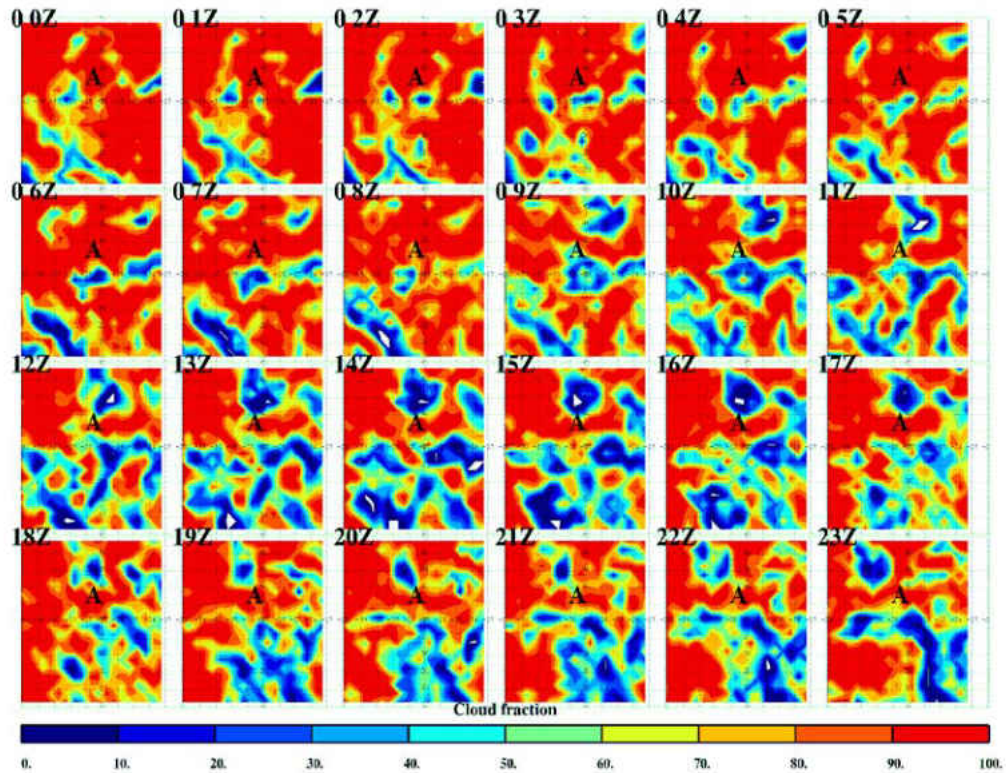


Figure 33. Hourly total cloud fraction images from Meteosat-9 over the Azores (A) on 14 October, 2010.

The days investigated in this case have similar cloud fraction trends. During the early morning hours, the stratocumulus layer remained unbroken for most of the days. The cloud layer would then begin to break apart during the afternoon hours, only to partially reform again in the evening hours. The coupled period in this case coincided with the early morning hours. These trends are consistent with other studies (Dong et al. 2014a, Wood 2012). The stratocumulus layer remained relatively unbroken during the night due to LW cooling at the cloud top being the dominant forcing. This LW cooling initiated a circulation that reached the surface and was able to provide the cloud layer a source of moisture. This is the reason why the coupled period coincided with the night/early morning hours of 12 October, 2010. During the day, however, SW heating at the cloud

top reduced the effect of LW cooling, which cut off the cloud layer's source of moisture causing the stratocumulus layer to break apart.

CHAPTER V

CONCLUSIONS

In this study, seven cases with coupled or decoupled stratocumulus clouds over the Azores were selected for study using the ARM AMF cloud radar and Meteosat-9 satellite imagery over the AMF-Azores site. It was found that when stratocumuli are coupled to the surface, they have low LWP, r_e , cloud thickness, and cloud top heights while decoupled periods have high LWP, r_e , and cloud thickness. These result primarily because decoupled periods have greater amounts of drizzle events (37%) compared to coupled periods (29%). It was also found that coupled periods had higher N_{CCN} and N_d values compared to decoupled periods because the decoupled stratocumulus layer has no source of surface aerosols and due to the significantly greater amount of drizzle events that occurred when stratocumuli were decoupled compared to coupled stratocumuli. The differences previously mentioned were also tested using the Student's T-Test and effective size. It was found that all of the differences mentioned are statistically significant and also have moderate or greater practical significance. Another finding was that the inversion layer for coupled periods was stronger, and lower compared to the decoupled periods, thus forcing the cloud layer to remain thin.

It was also found that coupled/decoupled drizzling stratocumuli have higher LWP, r_e , cloud thickness, and cloud top heights compared to coupled/decoupled non-drizzling stratocumuli. This finding is consistent with other studies (Woods 2005, Remillard et al. 2012). Coupled/decoupled non-drizzling stratocumulus clouds had higher

N_d and N_{CCN} values compared to coupled/decoupled drizzling stratocumulus clouds because drizzle depletes the amount of cloud condensation nuclei and cloud droplets within the stratocumulus cloud. The mean differences previously mentioned were also found to be statistically and practically significant. The differences in means for different micro-physical properties (except N_{CCN} and N_d) between non-drizzling/drizzling stratocumuli are larger compared to those for coupled/decoupled stratocumuli. This suggests that drizzle has a greater effect on micro-physical characteristics (except N_{CCN} and N_d) of stratocumuli than does coupling. N_{CCN} and N_d values, however, are more affected by the coupling or decoupling of the stratocumulus layer. There is some overlap between the LWP, N_d , r_e , and cloud thickness distributions of drizzling and non-drizzling stratocumuli because a portion of the drizzling stratocumuli produce only producing virga, and thus have very similar micro- and macrophysical characteristics as non-drizzling stratocumuli.

No significant differences existed between coupled stratocumuli that occurred during the day or night, due to night and day stratocumuli have relatively the same amount of drizzle samples 70% and 68%, respectively. Decoupled stratocumuli that occurred at nighttime tended to have higher LWP, cloud thickness, r_e values, and lower N_d values compared to daytime coupled stratocumuli, which suggests heavier drizzle was present during the night. It was also found that nighttime stratocumuli (33%) are more coupled compared daytime stratocumuli (19%).

Finally, by reviewing satellite imagery (Figs. 30-33) for the 11-14 October, 2010 case, it was determined that the stratocumulus layer was closed celled during the night and early morning, while broken during the afternoon. During the nighttime and early

morning, LW cooling is the dominant forcing at the cloud top, which helps sustain the circulation that supplies the stratocumulus layer with moisture. During the afternoon, SW heating at the cloud top suppresses the longwave cooling there, which weakens the circulation. The stratocumulus layer was coupled to the surface from 0:00-9:00 UTC on October 12, which coincided to a period when the stratocumulus layer was unbroken.

CHAPTER VI

REFERENCES

Chen, et al 2000: Radiative effects of cloud-type variations. *J. Climate*, **13**, 264-286.

Cohen, J., 1988: Statistical power analysis for the behavioral sciences (2. Auflage).

Hillsdale, NJ: Erlbaum.

Coulter, R., 2012: Micropulse Lidar (MPL) Handbook. DOE/SC-ARM/TR-019,

Department of Energy.

Dong X., T. P. Ackerman, and E. E. Clothiaux, 1998: Parameterizations of the microphysical and shortwave radiative properties of boundary layer stratus from ground-based measurements. *J. Geophys. Res. Atmos.*, **103**, 681-693.

Dong X., P. Minnis, T. P. Ackerman, E. E. Clothiaux, G. G. Mace, C. N. Long, and J.

C. Liljegren, 2000: A 25-month database of stratus cloud properties generated from

ground-based measurements at the Atmospheric Radiation Measurement Southern Great

Plains Site. *J. Geophys. Res. Atmos.*, **105**, 4529-4537.

Dong, X., and G. G. Mace, 2003: Profiles of Low-Level Stratus Cloud Microphysics Deduced from Ground-Based Measurements. *J. Atmos. Oceanic Technol.*, **20**, 42-53.

Dong X., B. Xi, A. Kennedy, P. Minnis and R. Wood, 2014a: A 19-Month Record of Marine Aerosol–Cloud–Radiation Properties Derived from DOE ARM Mobile Facility Deployment at the Azores. Part I: Cloud Fraction and Single-Layered MBL Cloud Properties. *J. Climate*, **27**, 3665-3682.

Dong X., B. Xi., and P. Wu, 2014b: Investigation of the diurnal variation of marine boundary layer cloud microphysical properties at the Azores. *J. Climate*.

Frisch, A. S., C. W. Fairall, and J. B. Snider, 1995: Measurement of stratus cloud and drizzle parameters in ASTEX with Ka-band Doppler radar and a microwave radiometer. *J. Atmos. Sci.*, **52**, 2788-2799.

Hahn, C. J., and S. G. Warren, 2007: A gridded climatology of clouds over land (1971-96) and ocean (1954-97) from surface observations worldwide. Numeric Data Package NDP-026E ORNL/CDIAC-153, CDIAC, Department of Energy, Oak Ridge, TN.

Hartmann, D. L., D. Short, 1980: On the use of earth radiation budget statistics for studies of clouds and climate. *J. Atmos. Sci.*, **31**, 1233-1250.

Hartmann, D. L., M. E. Ockert-Bell, and M. L. Michelsen, 1992: The effect of cloud type on earth's energy balance – Global analysis. *J. Climate*, **5**, 1281-1304.

Hartmann, D. L., 1994: *Global Physical Climatology*, Academic Press.

Holdridge, D., et al, 2011: Balloon-Borne Sounding System (SONDE) Handbook. DOE/SC-ARM/TR-029, Department of Energy.

Jefferson, A., 2011: Aerosol Observing System (AOS) Handbook. ARM-TR-014, Department of Energy.

Jenson, M. P., 2008: Investigation of Regional and Seasonal Variations in Marine Boundary Layer Cloud Properties from MODIS Observations. *J. Climate*, **21**, 4955-4973.

Jones, C., C. Bretherton, and D. Leon, 2011: Coupled vs. decoupled boundary layers in VOCALS-Rex. *Atmos. Chem. Phys.*, **11**, 7143-7153.

Kwon, B. H., B. Bénech, D. Lambert, P. Durand, A. Druilhet, H. Giordani, and S. Planton, 1998: Structure of the marine atmospheric boundary layer over an oceanic thermal front: SEMAPHORE experiment. *J. Geophys. Res. Atmos.*, **103**, 159-180.

Leon, D. C., Z. Wang, and D. Liu, 2008: Climatology of drizzle in marine boundary layer clouds based on 1 year of data from CloudSat and Cloud-Aerosol Lidar and Infrared Pathfinder Satellite Observations (CALIPSO). *J. Geophys. Res. Atmos.*, **113**, D00A14.

Liljegren J. C., 2001: A new retrieval for cloud liquid water path using a ground-based microwave radiometer and measurements of cloud temperature. *J. Geophys. Res. Atmos.*, **106**, 14485-14500.

Lilly, D. K., 1968: Models of cloud-topped mixed layers under a strong inversion. *Quart. J. Roy. Meteor. Soc.*, **94**, 292-309.

Logan, T., B. Xi, and X. Dong, 2014: Aerosol properties and their influences on marine boundary layer cloud condensation nuclei at the ARM mobile facility over the Azores. *J. Geophys. Res. Atmos.*, **14**.

Morris, V. R., 2006: Microwave Radiometer (MWR) Handbook. ARM TR-016, Department of Energy.

Miller, M. A., and B. A. Albrecht, 1995: Surface-Based Observations of Mesoscale Cumulus-Stratocumulus Interaction during ASTEX. *J. Atmos. Sci.*, **52**, 2809-2826.

Morris, V. R., 2012: Vaisala Ceilometer Handbook. DOE/SC-ARM-TR-020, Department of Energy.

Nicholls, S., J. Leighton, 1986: An observational study of the structure of stratiform cloud sheets: Part II. Entrainment. *Quart. J. Roy. Meteor. Soc.*, **112**,. 431-460.

Randall, D. A., J. A. Coakley, C. W. Fairall, R. A. Knopfli, and D. H. Lenschow, 1984: Outlook for research on marine subtropical stratocumulus clouds, *Bull. Amer. Meteor. Soc.*, **65**, 1290-1301.

Remillard, J., P. Kollias, E. Luke, and R. Wood 2012: Marine Boundary Layer Cloud Observations in the Azores. *J. Climate*, **25**, 7381-7397.

Slingo, A., 1990: Sensitivity of the Earth's radiation budget to changes in low clouds. *Nature*, **343**, 49-51.

Stephens, G. L., T. J. Greenwald, 1991: Observations of the Earth's radiation budget in relation to atmospheric hydrology. Part II: Cloud effects and cloud feedback. *J. Geophys. Res. Atmos.*, **96**, 15 325- 15 340.

Troyan, D., 2012: Merged Sounding Value-Added Product. DOE/SC-ARM/TR-087, Department of Energy.

Turton, J. D., S. Nicholls, 1987: A study of the diurnal variation of stratocumulus using a multiple mixed layer model. *Quart. J. Meteor. Soc.*, **113**, 969-1009.

Warren, S. G., C. J. Hahn, J. London, R. M. Chervin, and R. L. Jenne, 1986: Global distribution of total cloud cover and cloud types over land. NCAR Technical Note NCAR/TN-273+STR 29pp+200 maps, National Center for Atmospheric Research, Boulder, CO.

Warren, S. G., C. J. Hahn, J. London, R. M. Chervin, and R. L. Jenne, 1988: Global distribution of total cloud cover and cloud types over ocean, NCAR Tech. Note NCAR/TN-317+STR, National Center for Atmospheric Research, Boulder, CO, 42 pp. +170 maps.

Widener, K. B., K. Johnson, 2006: W-band ARM Cloud Radar (WACR) Handbook. ARM-TR-073, Department of Energy.

Wood, R., 2005: Drizzle in Stratiform Boundary Layer Clouds. Part I: Vertical and Horizontal Structure. *J. Atmos. Sci.*, **62**, 3011-3033.

Wood, R., 2005: Drizzle in Stratiform Boundary Layer Clouds. Part II: Microphysical Aspects. *J. Atmos. Sci.*, **62**, 3034-3050.

Wood, R., 2012: Review Stratocumulus Clouds. *Mon. Wea. Rev.*, **140**, 2373-2416.

Xi, B., and coauthors, 2014: Validation of CERES-MODIS Edition 4 Marine Boundary Layer Cloud Properties using DOE ARM AMF Measurements at the Azores. *J. Geophys. Res. Atmos.*, 55.